Controls on composition and diagenesis of wave- and river-dominated deltas: impacts on reservoir properties. An example from the La Anita Formation (Argentina)

Damián Moyano-Paz [a,b,*], Alejandro R. Gómez-Dacal [c,d], Augusto N. Varela [c,e], Marcos Comerio [c], Tobías M. Muñoz-Olivero [a], Joaquín Bucher [a], Sebastián Richiano [f], Daniel G. Poiré [a,d]

[a] Centro de Investigaciones Geológicas (CONICET-UNLP), Diagonal 113 #275, La Plata (1900), Buenos Aires, Argentina
[b] Cátedra de Sedimentología, Facultad de Ciencias Naturales y Museo. Universidad Nacional de La Plata, Argentina, Av. 60 esquina 122 s/n, La Plata, Argentina
[c] Y-TEC - YPF Tecnología S.A. and CONICET, Av. Del Petróleo s/n entre 129 y 143, Berisso, Buenos Aires, Argentina
[d] Cátedra de Rocas Sedimentarias, Facultad de Ciencias Naturales y Museo. Universidad Nacional de La Plata, Argentina, Av.60 esquina 122 s/n, La Plata, Argentina
[e] Cátedra de Micromorfología de Suelos, Facultad de Ciencias Naturales y Museo. Universidad Nacional de La Plata, Argentina, Av. 60 esquina 122 s/n, La Plata, Argentina
[f] CONICET – CENPAT Instituto Patagónico de Geología y Paleontología, Boulevard Brown 2915, 920, Puerto Madryn, Chubut, Argentina

ARTICLE INFO

ABSTRACT

Wave-, tidal-, and fluvial-dominated deltas are important hydrocarbon reservoirs worldwide, and it is well known that depositional facies types, detrital composition and diagenetic products are key aspects when evaluating potential reservoir properties. Moreover, detrital composition and diagenetic products are controlled by external forces such as tectonism, climate, and depositional conditions.

The Upper Cretaceous La Anita Formation (Austral-Magallanes Basin, Argentina) is a deltaic succession that shows a clear vertical variation in the relative role of wave, tidal and fluvial processes. The formation was accumulated during the foreland stage of the basin under relatively warm climate conditions. A detailed compositional and diagenetic analysis for these deposits is provided to evaluate the role of the controlling factors on the detrital and authigenic composition, and the impact on reservoir properties.

Samples were analyzed by conventional petrography, X-ray diffraction and scanning electron microscopy to obtain a full spectrum of its detrital, authigenic and diagenetic composition. The analyzed sandstones were classified as lithic arenites which come from the fold-thrust belt region and from the magmatic arc located toward the westward. The clay mineral composition is characterized by variable proportions of illite, smectite, kaolinite and mixed-layer illite-smectite with the sporadic presence of chlorite. Stratigraphic variations in the abundance of authigenic kaolinite and smectite indicate a change in the climatic conditions during the depositions of the unit evolving from tropical to more temperate conditions. Diagenetic processes affecting the porosity are considered as controlled mainly by the lithological nature of the deposits and depositional facies type. Sandstone porosity is mainly primary in origin, moderate to good in abundance and show micropore to mesopore as the main pore-sizes.

This work enhances that the diagenetic products are heavily controlled by the dominant depositional process. The presence of diagenetic products as quartz overgrowth and calcite and hematite cement reduces pore spaces and affects the reservoir properties. The development of these types of cement is conditioned by the relative dominance of wave and river processes. Under wave-dominated conditions, quartz tends to develop thick overgrowths. Conversely, under river-dominated conditions quartz overgrowths are thinner and calcite and hematite cementation patches are developed.

* Corresponding author:
  E-mail address: dmoyanopaz@cig.museo.unlp.edu.ar (D. Moyano-Paz).

1. Introduction

Detrital and authigenic compositional studies are useful for analyzing the evolution of sedimentary basins since they show temporal and spatial variations in the input of terrigenous clastic components coming from different source areas, tectonic configurations, climate conditions and degree of diagenesis, among others (Dickinson and Rich, 1972; Ingersoll, 1983; Critelli and Ingersoll, 1995; Cavazza and Ingersoll, 2005; Gómez-Peral et al., 2011; Varela et al., 2013, 2018). Sandstone petrography in clastic successions combined with paleocurrent data provides a well-established methodology for provenance, paleogeographic and basin analysis (Dickinson and Suczek, 1979; Zattin et al., 2003; Stefani et al., 2007; Varela et al., 2013).

The composition of whole rock and clay fraction will depend not only on the positive areas that supply clastic material but also on other factors such as depositional environments, transport mechanisms, climate, and diagenesis (Net et al., 2002; Gómez-Peral et al., 2011; Varela et al., 2018). Clay mineral assemblages are commonly studied by X-ray diffraction (XRD) and scanning electron microscopy (SEM) and represent the product of weathering and authigenesis that result of the interaction of different variables such as source area, basin morphology, depositional conditions and climate (Chamley, 1989; Do Campo et al., 2010; Richiano et al., 2015).

Diagenetic analyses via standard petrography and SEM are employed with success to predict reservoir quality in hydrocarbon exploration (e. g., Zhang et al., 2009; Morad et al., 2010; Taylor et al., 2010; Henares et al., 2016) since diagenetic processes control the development of porosity and permeability. Cementation, pressure solution, compaction and the authigenic clay content are the main pore volume-controlling factors, whereas cement dissolution and fracturing are the most important porosity-enhancing factors (Nabawy and Geraud, 2015).

Wave-, tidal-, and river-dominated deltaic deposits may not show significant differences in their detrital composition under the same relative influence of tectonic and climatic conditions. However, the diagenetic products recorded in different types of deltas could be slightly different and these impact on reservoir properties. In many cases, the difference in the behavior between detrital composition and diagenetic products can be explained through the depositional facies type (e.g., Morad et al., 2000, 2010; Bjørlykke, 2014; Lai et al., 2018).

The La Anita Formation (LAF) is a deltaic reservoir analog which shows clear vertical variations on the role of wave fluvial and tidal processes (e.g., Moyano-Paz et al., 2018, 2020). Also, this unit is a proven tight type of reservoir (Jait et al., 2018), providing a challenging opportunity to assess the relationship between detrital composition, the role of the relative dominance of the depositional processes and the diagenetic products with the resultant reservoir properties.

The aims of this study are: i) to evaluate compositional variations as response to the main compositional controls, ii) to assess the influence of relative dominance of wave and river processes on the development of different diagenetic products, and iii) to establish linkages between
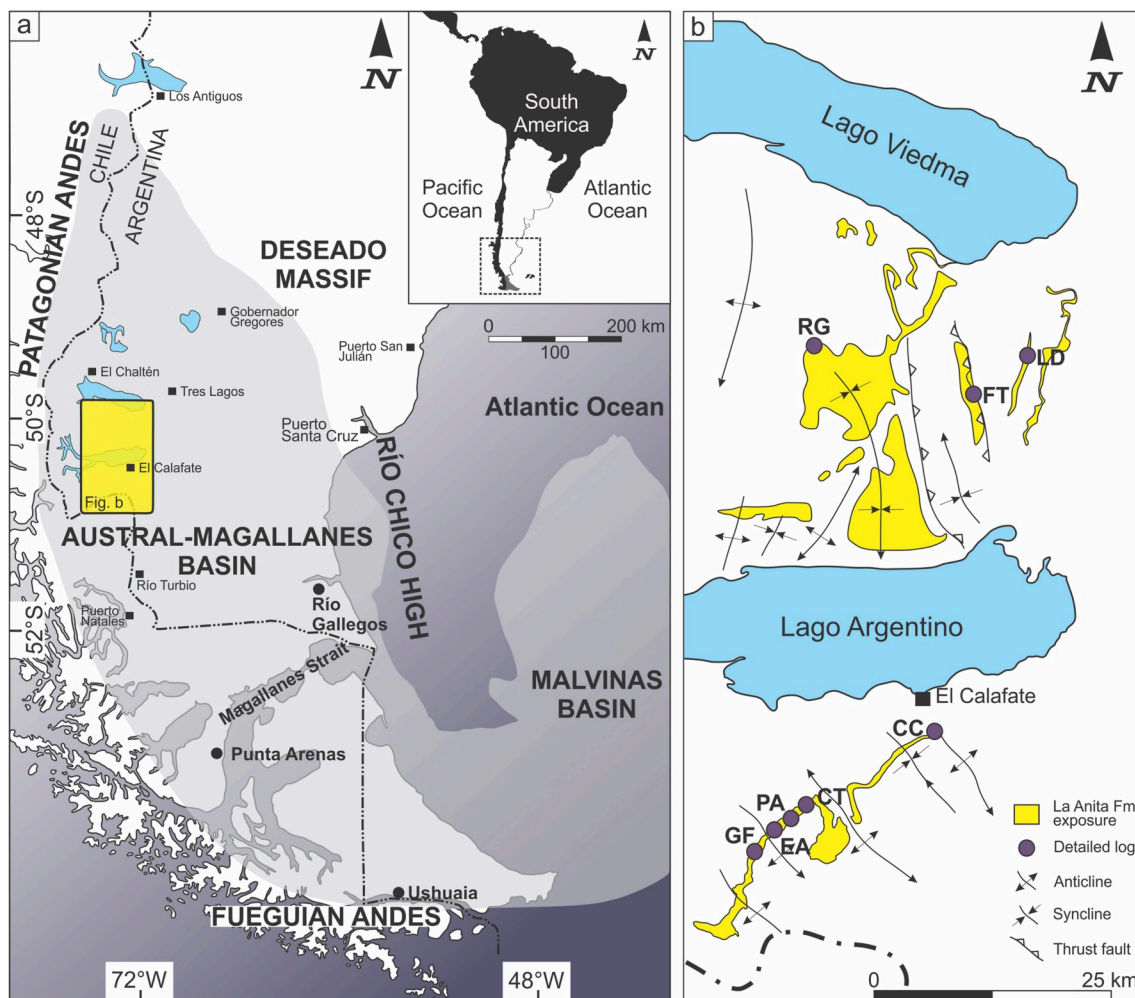

Fig. 1. Study area. a) General location of the AMB at southernmost Argentina and Chile. b) Detail map of the LAF exposures and location of detailed logs. Samples were collected in order to analyze the composition and diagenesis of the LAF. RG = Río Guanaco; GF = Galpón de Freile; EA = Estancia Anita; CT = Campo Tropilla; CC = Cerro Calafate; LD = Luz Divina; FT = Filo del Turbio; PA= Paredón.

detrital composition and diagenetic products to analyze the impact on potential reservoir properties as a predictive tool.

2. Geological background

The Austral-Magallanes Basin (AMB) is located at the southernmost end of Patagonia and is one of the most important oil- and gas-producing sedimentary basins of Argentina and Chile (Fig. 1). The tectonic history of the basin is characterized by three main stages (Biddle et al., 1986): a rift stage, a postrift thermal subsidence stage and finally, a foreland stage.

The transition from extensional to compressional regime took place ~100 Ma and marks the beginning of the foreland stage (Biddle et al., 1986; Fosdick et al., 2011; Varela et al., 2012; Ghiglione et al., 2015; Malkowski et al., 2017). Shortening caused during the early stages of the orogeny resulted in a retroarc fold-thrust belt along the Patagonian-Fuegian Andes (Fildani and Hessler, 2005; Fosdick et al., 2011; Varela et al., 2012, 2013) which is associated along its eastern margin with the AMB foreland system.

The onset of the foreland regime is recorded by flexural deeping of the foredeep main depozone from 100-500 m to 1000–2000 m (Natland et al., 1974). The AMB foreland system is characterized by a thick marine infill followed by continental deposits, representing an evolution

from an underfilled to overfilled stage (Malkowski et al., 2015; Tettamanti et al., 2018; Moyano-Paz et al., 2018, 2020, 2022; Varela et al., 2019; Ghiglione et al., 2021, Fig. 2). Sediment accumulation in the foredeep starts with the deep-marine, siliciclastic, turbiditic deposits of the Cerro Toro Formation (Albian-Cenomanian; Wilson, 1991; Fildani and Hessler, 2005; Malkowski et al., 2015, 2017), which are covered by the siliciclastic fine-grained, prograding slope to outer-shelf deposits of the Alta Vista/Tres Pasos Formation (Hubbard et al., 2010; Daniels et al., 2018, 2019). This deep-marine sedimentation is capped on top by the Santonian-Maastrichtian siliciclastic coastal deposits of the La Anita Formation or by its equivalent in Chile, the Dorotea Formation (Macellari et al., 1989; Moyano-Paz et al., 2018, 2020; Santamarina et al., 2020; Ghiglione et al., 2021). Finally, this marine succession is overlain by the uppermost Cretaceous continental deposits, which include several lithostratigraphic units such as the Cerro Fortaleza, La Irene and Chorrillo formations (Fig. 2; Tettamanti et al., 2018; Ghiglione et al., 2021; Moyano-Paz et al., 2022).

The Upper Cretaceous LAF (Bianchi, 1967) consists of a siliciclastic sandstone-dominated deltaic-coastal unit (e.g., Manassero, 1988; Moyano-Paz et al., 2018). The LAF is divided into two informal units: the lower unit and the upper unit, which are limited by a sequence boundary (*sensu* Moyano-Paz et al., 2018, Fig. 2). The lower unit is composed mainly of grayish fine-to coarse-grained sandstone with subordinate
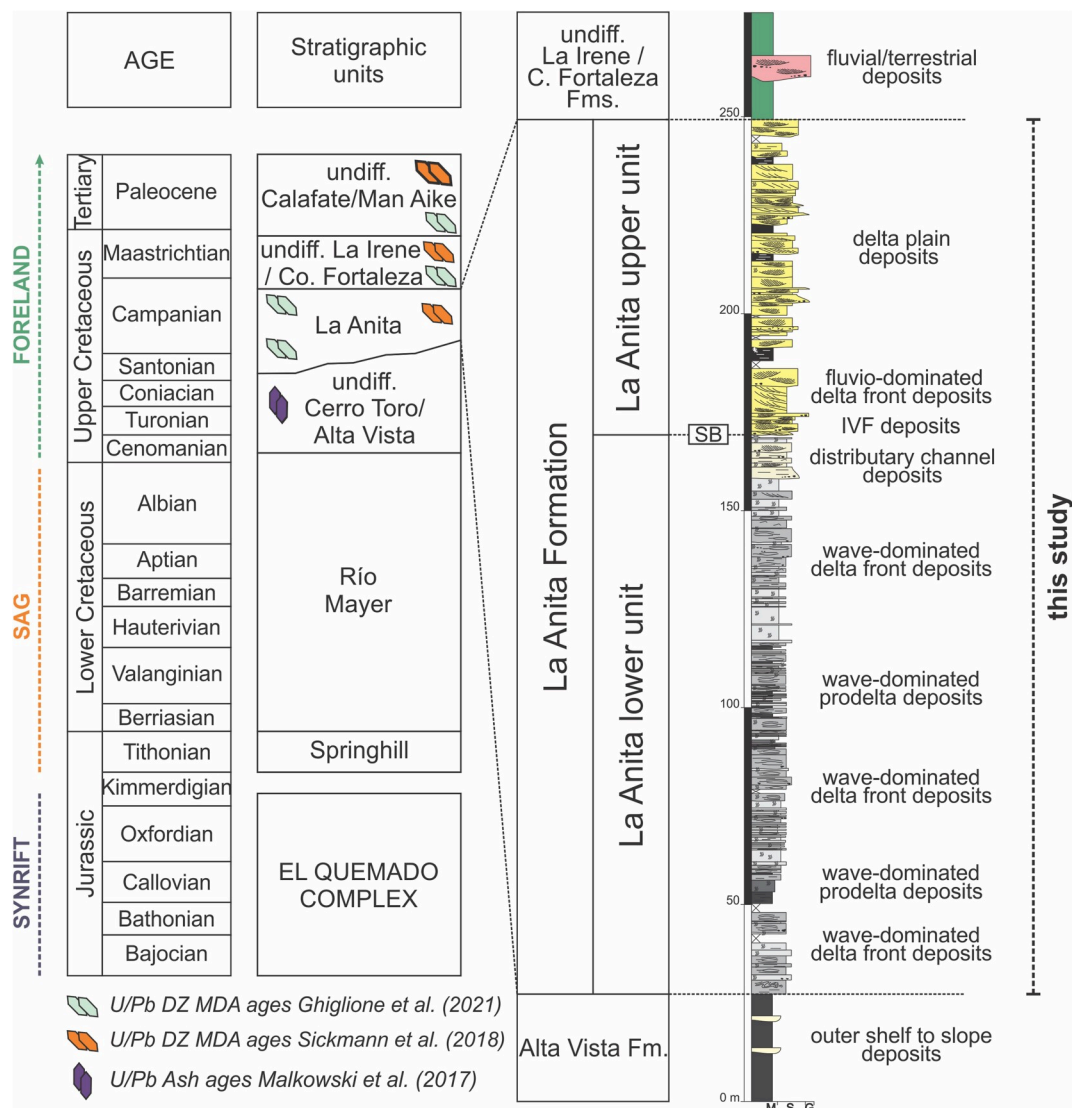

Fig. 2. Stratigraphic chart for the AMB in the Lago Argentino region and detail of stratigraphy and facies of the La Anita Formation.

participation of mudstones, heterolithic deposits and fine-grained conglomerates, it shows aggradational to progradational vertical stacking patterns and is interpreted as accumulated in a storm wave-dominated, river-influenced deltaic depositional system (Moyano-Paz et al., 2018, 2020). Conversely, the upper unit is divided into two intervals, the lowermost interval shows the coarser grain-sizes of the formation, including coarse-grained conglomerates to coarse-grained sandstones and is interpreted as the fluvial infill of an incised valley (Moyano-Paz et al., 2018). The uppermost interval of the upper unit is composed of fine-grained sandstones to pebbly-sandstones displaying heavily progradational stacking patterns and is interpreted as the accumulation in a river-dominated, tidal-influenced delta system (Moyano-Paz et al., 2020).

3. Methods

3.1. Fieldwork

Eight sedimentary sections were described in detail for the LAF deposits in different localities in the Lago Argentino region, five sections located to the south and three sections to the north of the lake (Fig. 1). Paleocurrent data (n = 375) were measured from current ripples and trough, tangential and planar cross-bedded structures using a Brunton® compass following the criteria of DeCelles et al. (1983) and Bossi (2007). Paleocurrent directions were corrected for magnetic declination according to the date on which they were surveyed. Data were grouped according to the facies association following the previous division of Moyano Paz et al. (2018).

Samples were collected in order to analyze the composition and diagenesis of the LAF. Sampling was carried out in five localities, one to the north of the Lago Argentino (RG = Río Guanaco), and four to the south (GF = Galpón de Freile; EA = Estancia Anita; CT = Campo Tropilla; and CC = Cerro Calafate). Sampled rocks were siliciclastic mudstones and fine-to medium-grained sandstone, in order to detect the greatest possible variability.

3.2. Petrography

Twenty-seven samples of sandstone (Table 1; eight from GF, eleven from CT and eight from CC) were analyzed by conventional petrography using Nikon Eclipse E−200 in order to analyze detrital components and diagenetic products and processes. For each sample, four hundred components were counted using a Swift point counter following the Gazzi-Dickinson methods to minimize the effect on the grain size on the modes (Gazzi, 1966; Dickinson, 1970; Ingersoll et al., 1984). Detrital modes were used to classify the sandstones according to Folk et al., (1970) and Dott (1964), modified by Pettijohn et al. (1972). For discrimination and discussion of sandstone provenance QpLvLs, QmFLt, and QtFL ternary diagrams of Dickinson and Suczek (1979), Dickinson et al. (1983) and Dickinson (1988) were used following the Zahid and Barbeau (2011) plotting criteria. The optical abundance and size of pore spaces was estimated following the criteria proposed by Net and Limarino (2000). Pore-rugosity was estimated qualitatively from thin sections depending on the presence and type of cements, clay precipitation and distribution of dissolution.

3.3. X-ray diffraction (XRD)

A total of eighty-two sandstones and mudstones samples (Table 2; thirteen from RG, twenty-one from GF, sixteen from EA, fourteen from CT and eighteen18 from CC) were prepared for whole rock and clay fraction (<2 μm) XRD analysis. Samples were subjected to soft grinding with a rubber mortar and repeatedly washed in distilled water until deflocculation occurred. XRD patterns from randomly oriented mounts (whole rock) of powdered samples were run from 0 to 37°2θ for 3 h on an X PANanalytical model X'Pert PRO diffractometer using Cu/Ni radiation and generation settings of 40 kV and 40 mA.

Semi-quantification of mineralogical components from the whole-

Table 1
Recalculated point-count data for the La Anita Formation sandstones.

Un.	Loc.	Sample	Detrital components %										%M	%C	%P	Qt	Qm	F	L	Lt
			Qm	Qp	Plg	Fk	Lv	Ls	Lm	PMz	Phy								
lu	GF	GF 5	23.5	10.5	3.5	8.5	43	3	2	–	5.75	0.25	3.25	12	35.9	25.3	11.2	52.8	63.5
lu	GF	GF 23	20.2	7.1	4.2	5.2	50.7	3.7	1.7	–	7.1	1.21	0.75	12	29.6	22.5	8.3	62.13	69.2
lu	GF	GF 38	19.8	7.8	2.6	5.2	52.7	3.4	1.15	–	7.2	1.44	4.5	12	29.8	21.4	8.4	61.8	70.2
lu	GF	GF 99	22.4	12.7	1.9	6.3	47.9	1.7	–	–	6.9	0.8	0.55	12	37.8	24.1	8.9	53.3	66.9
lu	GF	GF 107	22.6	9.7	2.4	5.9	49.3	2.2	0.5	–	7.3	0.8	5	5	34.9	24.4	9	56.1	66.6
lu	GF	GF 216	24.1	7.8	3.2	6.1	48.7	2.6	1.4	–	6.1	1.2	0.8	12	33.9	25.6	9.9	56.2	64.5
lu	GF	GF 264	22.1	6.3	4.5	9.3	48.8	1.5	1.2	–	6.3	3.9	0.9	20	30.3	23.6	14.7	54.9	61.7
uu	GF	GF 326b	26.3	10.6	4.8	3.6	48	2.1	1.5	–	3	3	1.8	15	38	27.1	8.7	53.3	64.2
lu	CT	CT 3	27.5	6.1	3.2	9.6	44.7	3.5	1.3	–	4.1	0	1.2	20	35	28.7	13.3	51.7	58
uu	CT	CT 85	24.6	7.9	3.5	5.3	50	2.9	0.6	–	5.2	0.6	14.6	10	34.3	25.9	9.3	56.5	64.8
uu	CT	CT 102	21.1	7.4	4.6	6.6	51.8	2.6	1.4	–	5.3	2.3	7.5	7	29.8	22.1	11.6	58.5	66.2
uu	CT	CT 115	24.5	11	4.6	5.2	46.1	1.7	1.2	–	6.7	2	5.2	9	36.9	25.1	10.6	52.5	64.3
uu	CT	CT 128	20.3	7.9	3.2	6.5	49.4	3.5	1.8	–	7.3	2	5.5	10	30.5	21.9	10.5	59	64.3
uu	CT	CT 143	21.8	6.6	4.6	8.9	50.4	2.3	–	–	5.4	2	4.8	5	30	23	14.2	55.8	62.7
uu	CT	CT 156	23	10	2	6.6	49.3	1.7	1.7	1.1	4.3	5	1.7	15	35.1	24.4	9.1	55.8	66.5
uu	CT	CT 159	21.4	8.4	4.9	5.8	46.8	2.9	2.6	1.73	5.49	3.5	6	15	32.1	23.1	11.5	56.4	65.4
uu	CC	CC 1	18.9	6.2	4	9.9	49.3	4	0.8	–	6.7	2.7	2	5	26.9	20.2	15	58.1	64.7
uu	CC	CC 2	15.7	9	4.1	7.7	50.27	3.6	1.9	–	7.7	3	2	5	26.8	16.7	12.8	60.4	70.2
uu	CC	CC 3	18.9	5.2	2.2	7.3	54.3	3.2	1.2	–	6.6	2	7	7	25.8	20.2	11.2	62.9	68.5
uu	CC	CC 4	17.3	5.7	4.8	6.9	54.8	2.9	1.5	–	7	3.9	5	10	24.5	18.5	12.4	64.1	69.1
uu	CC	CC 5	20.3	7.4	1.9	6.6	53.3	2.2	1.9	–	6.3	1.4	5.8	10	29.6	21.7	9.1	61.3	69.2
uu	CC	CC 6	22.8	7.4	2.6	6.3	53.6	2.3	0.6	–	4.5	1.4	5	10	31.6	23.9	9.3	59.1	66.9
uu	CC	CC 7	21.6	4.5	2.7	7.8	52.2	3.6	1.5	–	6	2.4	14	5	27.8	23	11.2	61	65.8
uu	CC	CC 8	21.4	4.3	2.6	5.1	54	3.1	1.7	–	7.7	3.7	7	7	27.9	23.2	8.4	63.8	68.4
uu	CC	CC 9	18.3	5.8	3.3	8	53.6	4.1	1.6	–	5	1.1	2	7	25.4	19.3	12	62.6	68.7
uu	CC	CC 10	25.3	5.9	3.2	9.1	4.742.6	4.7	2.9	–	6.2	1.1	1.5	10	33.2	26.9	13.2	53.6	59.9
uu	CC	CC 11	26.4	5.7	5	5.3	49.4	2.8	1.8	–	3.5	2	15	2	33.2	27.4	10.7	56	61.9

Abbreviations: Un. = Unit; Loc. = Locality; Qm = monocrystalline quartz; Qp = polycrystalline quartz; Plg = plagioclase; Fk = pottasium feldspar; Lv = volcanic lithic; Ls = sedimentary lithic; Lm = metamorphic lithic; PMz = pseudomatrix; M = matrix; C = cement; P = porosity; Pms = porosity mean size; Qt = Qm + Qp; F = Fk + Plg; L = Lv + Ls + Lm; Lt = L + Qp; lu = lower unit; uu = upper unit.

TABLE 2a
X-ray Diffraction data of the La Anita Formation.

Un.	Loc.	Sample	Lithol.	Whole Rock												Clay fraction				
				Q	FK	Pl	Ca	D	S	Cli	A	Ht	Mg	Clays	I	Cl	K	I/S	Sm
lu	EA	EA 2	Sand	72	5	10	–	1	–	–	–	–	–	12	50	0	25	25	0
lu	EA	EA 37	Sand	89	1	6	–	–	–	–	–	–	–	4	30	0	45	25	0
lu	EA	EA 44	Sand	73	8	13	–	–	–	–	–	–	–	6	40	10	35	10	5
lu	EA	EA 81	Sand	82	3	10	–	–	–	–	–	–	–	5	30	10	50	25	0
lu	EA	EA 87	Sand	70	6	15	–	–	–	–	–	–	–	9	60	5	10	25	0
lu	EA	EA 96	Sand	66	3	8	–	–	–	–	–	–	–	23	35	0	5	60	0
lu	EA	EA 98	Sand	74	5	15	–	–	–	–	–	–	–	6	25	25	35	15	0
uu	EA	EA 110	Sand	72	6	15	–	2	–	–	–	–	–	5	30	30	30	10	0
uu	EA	EA 118	Sand	83	3	10	–	–	–	–	–	–	–	4	40	20	15	25	0
uu	EA	EA 130	Sand	82	4	9	–	1	–	–	–	–	–	4	40	20	20	15	5
uu	EA	EA 147	Sand	79	3	15	–	–	–	–	–	–	–	3	60	0	5	30	5
uu	EA	EA 149c	Sand	88	4	6	–	–	–	–	–	–	–	2	60	0	10	30	0
uu	EA	EA 157a	Mud	84	3	6	–	–	–	–	–	–	–	7	40	35	5	20	0
uu	EA	EA 157c	Mud	50	2	6	11	1	–	–	–	–	–	30	35	0	10	35	20
uu	EA	EA 175	Mud	77	3	5	–	–	–	–	–	–	–	15	35	15	5	35	10
uu	EA	EA 178	Sand	88	1	6	–	–	–	–	–	–	–	5	35	5	50	15	0
lu	GF	GF 2	Sand	85	2	9	–	–	–	–	–	–	–	4	15	10	70	5	0
lu	GF	GF 10	Sand	75	5	8	5	2	–	–	–	–	–	5	15	10	70	5	0
lu	GF	GF 19	Sand	78	2	11	–	3	–	–	–	–	–	6	25	10	50	15	0
lu	GF	GF 23	Sand	83	4	4	2	2	–	–	–	–	–	5	20	10	65	5	0
lu	GF	GF 31	Mud	76	4	8	2	–	–	–	–	–	–	10	50	10	10	30	0
lu	GF	GF 33	Mud	79	4	5	2	2	–	–	–	–	–	8	30	20	30	20	0
lu	GF	GF 34	Mud	86	3	7	–	–	–	–	–	–	–	4	45	25	15	15	0
lu	GF	GF 35	Mud	79	2	9	–	1	–	–	–	–	–	9	35	15	40	10	0
lu	GF	GF 48	Sand	83	4	9	–	1	–	–	–	–	–	3	20	10	60	10	0
lu	GF	GF 63	Sand	74	7	8	–	1	–	–	–	–	–	10	30	10	50	10	0
lu	GF	GF 91	Sand	74	4	13	–	1	–	–	–	–	–	8	25	15	50	10	0
lu	GF	GF 129	Mud	75	3	8	–	1	–	–	–	–	–	13	35	15	25	20	5
lu	GF	GF 185	Mud	78	3	12	–	–	–	–	–	–	–	7	30	15	30	20	5
lu	GF	GF 187	Sand	68	4	6	–	2	–	–	–	–	–	20	30	25	5	30	10
lu	GF	GF 282	Sand	82	2	7	–	–	–	–	–	–	–	9	30	25	25	20	0
uu	GF	GF 309	Mud	79	2	13	–	–	–	–	–	–	–	6	35	15	25	15	10
uu	GF	GF 310	Sand	75	3	8	–	–	–	–	–	–	–	14	45	0	10	35	10
uu	GF	GF 346b	Mud	88	3	7	–	–	–	–	–	–	–	2	60	0	40	0	0
uu	GF	GF 360	Mud	84	3	8	–	–	–	–	–	–	–	5	35	45	15	5	0
uu	GF	GF 385	Sand	88	3	4	–	–	–	–	–	–	–	5	35	0	30	20	5
uu	GF	GF 398	Sand	77	6	8	–	–	–	–	–	–	–	9	25	35	25	10	5
lu	CT	CT 3	Sand	70	5	5	15	–	–	–	–	–	–	5	15	10	40	35	0
lu	CT	CT 21	Sand	30	5	10	45	–	–	–	–	–	–	10	30	10	25	25	5
lu	CT	CT 60	Sand	80	5	10	–	–	–	–	–	–	–	5	25	25	5	45	0
uu	CT	CT 85	Sand	88	2	8	–	–	–	–	–	–	–	2	10	0	0	90	0
uu	CT	CT 102	Sand	80	3	15	–	–	–	–	–	–	–	2	20	20	10	50	0
uu	CT	CT 105	Sand	84	3	10	–	–	–	–	–	–	–	3	25	10	5	60	0
uu	CT	CT 108	Sand	89	3	6	–	–	–	–	–	–	–	2	15	20	5	40	20
uu	CT	CT 128	Mud	92	1	4	–	–	–	–	–	–	–	3	20	2	10	65	0
uu	CT	CT 131	Sand	67	4	5	–	–	–	–	–	–	–	24	5	0	10	65	20
uu	CT	CT 143	Mud	75	5	14	–	–	–	–	–	–	–	6	50	0	5	45	0
uu	CT	CT 150	Sand	71	4	7	–	–	–	–	–	–	–	18	20	0	5	75	0
uu	CT	CT 156	Sand	76	10	9	–	–	–	–	–	–	–	5	20	15	5	60	0
uu	CT	CT 159	Sand	84	3	9	–	–	–	–	–	–	–	4	15	20	30	35	0
uu	CT	CT 170	Sand	82	3	11	–	–	–	–	–	–	–	4	15	30	25	30	5

Abbreviations: Q = quartz, FK = potassium feldspar, Pl = plagioclase, Ca = calcite, D = dolomite, S = siderite, A = analcime, Ht = hematite, Mg = magnetite, I = illite, Cl = chlorite, K = kaolinite, I/S = illite-smectite, Sm = smectite.

rock diagrams was obtained from the intensity of the main peak for each mineral (Schultz, 1964; Moore and Reynolds, 1997) and classified according to the following abundances: traces (<1%); very scarce (1–5%); scarce (5–20%); moderate (20–40%); abundant (40–60%); and very abundant (>60%).

The <2 μm fraction was separated by gravity settling in suspension, and oriented mounts were prepared on glass slides. Clay mineralogy was determined from diffraction patterns obtained using samples that were air-dried, ethylene glycol-solvated, and heated to 550 °C for 2 h (Brindley, 1961; Brown, 1980). Routine air-dried mounts were run between 2 and 32°2θ at a scan speed of 2°2θ/min. Ethylene glycol-solvated and heated samples were run from 2 to 27°2θ and 3–15°2θ, respectively, at a scan speed of 2°2θ/min. Semi-quantitative estimations of the relative concentrations of clay minerals were based on the peak area method (Biscaye, 1965) on natural or glycolated samples given the absence or presence of smectite and/or mixed-layers chlorite-smectite and illite-smectite. Relative percentages of each clay mineral were determined by applying empirical factors following the Moore and Reynolds (1989) criteria.

The abundance of different mineralogical components and clay minerals obtained from whole rock and clay fraction analysis is summarized in Table 2.

3.4. Scanning electron microscope (SEM)

Three samples of sandstone (one from GF, one from CT and one from CC) were selected considering the position in the sedimentary log, the presence of clays and diagenetic products. Chips were covered with Au and analyzed by SEM under secondary electron and backscattered diffraction modes with Energy Dispersive X-ray Spectroscopy using an

TABLE 2b
X-ray Diffraction data of the La Anita Formation.

Un.	Loc.	Sample	Lithol.	Whole Rock											Clay fraction				
				Q	FK	Pl	Ca	D	S	Cli	A	Ht	Mg	Clays	I	Cl	K	I/S	Sm
uu	CC	CC 1	Sand	82	7	5	1	–	–	–	–	–	–	5	10	5	85	0	0
uu	CC	CC 2	Sand	87	7	2	–	–	–	–	–	–	–	4	5	5	90	0	0
uu	CC	CC 3	Sand	86	7	2	–	0	–	–	–	–	–	5	10	5	85	0	0
uu	CC	CC 4	Sand	80	8	4	–	1	–	–	–	–	–	7	15	10	60	15	0
uu	CC	CC 5	Sand	84	6	3	1	1	–	–	–	–	–	5	10	5	85	0	0
uu	CC	CC 6	Sand	89	5	3	1	–	–	–	–	–	–	2	15	5	75	5	0
uu	CC	CC 7	Sand	84	8	4	–	–	–	–	–	–	–	4	30	5	60	5	0
uu	CC	CC 8	Sand	84	3	2	–	–	–	–	–	–	–	1	10	0	85	5	0
uu	CC	CC 9	Sand	84	5	5	–	–	–	–	–	–	–	5	5	0	85	10	0
uu	CC	CC 10	Sand	84	3	2	1	–	–	–	–	–	–	1	5	0	95	0	0
uu	CC	CC 11	Sand	84	4	2	6	–	–	–	–	–	–	4	5	0	90	5	0
uu	CC	CC Ca 2	Mud	84	5	2	2	–	–	–	–	–	–	16	25	0	20	35	20
uu	CC	CC Ca 13	Mud	84	6	5	0	–	–	–	–	–	–	27	15	0	20	35	30
uu	CC	CC Ca 25	Mud	84	2	2	2	–	–	–	–	–	–	9	40	0	30	20	10
uu	CC	CC Ca 30	Sand	84	3	1	0	–	–	–	–	–	–	1	0	0	90	10	0
uu	CC	CC Ca 50	Mud	84	2	2	2	–	–	–	–	–	–	16	30	0	30	20	20
uu	CC	CC Ca 58	Mud	84	4	2	0	–	–	–	–	–	–	38	15	0	10	20	60
uu	CC	CC Ca 64	Mud	84	2	2	2	–	–	–	–	–	–	31	20	0	15	35	30
lu	RG	RG-10	Mud	84	2	13	1	–	–	–	–	–	–	8	15	10	50	25	0
lu	RG	RG-34	Mud	84	2	4	–	–	–	–	–	–	–	35	15	0	5	80	0
lu	RG	RG-41	Sand	84	3	12	6	–	–	–	–	–	–	8	15	5	30	50	0
lu	RG	RG-45	Sand	84	4	13	6	–	–	–	–	–	–	8	15	5	35	45	0
lu	RG	RG-59	Sand	84	2	14	0	–	–	–	–	–	–	4	15	5	35	45	0
lu	RG	RG-65	Sand	84	13	8	–	–	–	–	–	–	–	6	20	5	40	35	0
lu	RG	RG-66	Sand	84	4	23	5	1	–	–	–	–	–	8	5	5	25	65	0
lu	RG	RG-67	Sand	84	3	7	–	1	–	–	–	–	–	18	5	20	0	80	0
lu	RG	RG-77	Sand	84	5	22	2	–	–	–	–	–	–	8	25	0	20	55	0
lu	RG	RG-93	Sand	84	2	17	1	1	–	–	–	–	–	4	15	0	35	50	0
uu	RG	RG-101	Sand	84	2	12	10	–	–	–	–	–	–	5	15	0	85	0	0
uu	RG	RG-107	Mud	84	2	8	–	–	–	–	–	–	–	9	15	10	10	65	0
uu	RG	RG-127	Sand	84	0	18	–	–	–	–	–	–	–	9	5	0	55	10	30

Abbreviations: Q = quartz, FK = potassium feldspar, Pl = plagioclase, Ca = calcite, D = dolomite, S = siderite, A = analcime, Ht = hematite, Mg = magnetite, I = illite, Cl = chlorite, K = kaolinite, I/S = illite/smectite, Sm = smectite.

FEI Quanta 200 SEM (Laboratorio de Investigaciones de Metalurgia Física, Universidad Nacional de La Plata, Argentina). The accelerating voltage was 20 kV with a current emission of 50–100 pA. This methodology was used to determine the clay origin and observe the cement morphology, pore geometry and diagenetic relationships.

4. Paleocurrent data

Paleocurrent data obtained from the wave-dominated, river-influenced delta of the lower unit were measured in the mouth-bars and both, terminal and distributary channels deposits (Fig. 3a and b). For the upper unit of the LAF, paleocurrent directions were measured in the amalgamated channel deposits of the incised valley fluvial infill (Fig. 3a and c) and the mouth bars and distributary channels of the river-dominated, tidal-influenced delta (Fig. 3a and d).

4.1. Lower unit

Paleocurrent measurements from the wave-influenced mouth-bar deposits show low data dispersion and indicate a mean paleoflow direction towards the northeast (Fig. 3a). The non-amalgamated terminal distributary channels show low direction dispersion and a mean paleoflow direction toward the southeast (Fig. 3a). The amalgamated distributary channels also flowed towards the southeast showing higher data dispersion (Fig. 3a).

4.2. Upper unit

The paleocurrent directions measured from the amalgamated fluvial deposits that filled the incised valley of the lowermost interval of the upper unit reflect that these channelized bodies flowed mainly toward the southeast (Fig. 3b). Flow directions measured from the river-dominated, tidal-influenced deposits show main directions towards the southeast and show higher dispersion than those measured from the wave-dominated delta (Fig. 3c).

5. Sandstone petrography

The LAF sandstones (n = 27; Table 1) are composed of siliciclastic detrital grains (75–93%, with an average of 85%), pores (2–20%, with an average of 10%) and authigenic cements (0.8–15%, with an average of 6%).

Petrographic analysis allowed the recognition of five main detrital components in the analyzed sandstone thin sections which are, in order decreasing of abundance: lithic fragments, monocrystalline quartz, polycrystalline quartz, feldspars and phytodetritus (terrestrial plant remains). These sandstones are clast supported with scarce participation of fine-grained muddy matrix, ranging between 0.25% and 4.5% (Table 1). The grain size of detrital components varies from very fine-to very coarse-grained sand. These components are subrounded to subangular and they are poor to well sorted.

Pore types recorded in the LAF sandstones are mainly primary in origin with the subordinate presence of secondary pores related to microfractures and dissolution. Dominant pore textures are intergranular and subordinate oversized, moldic and intragranular, in decreasing order of abundance (Fig. 4a–e). The dominant pore-sizes are micropore to mesopore (4–62 μm and 62–250 μm, respectively; *sensu* Net and Limarino, 2000), and eventually macropores (250–1000 μm). Pore-size sorting is mainly poor to moderate, and the dominant distribution is homogeneous to heterogeneous (Fig. 4a). The pore-rugosity is moderate to high, related to the presence of bitumen and clays as pore lining (Fig. 4e). The pore abundance in the sandstones of the LAF lower unit is higher than the ones recorded for the upper unit with porosity mean values of 13% (good) and 8.5% (moderate), respectively (Table 1; *sensu*
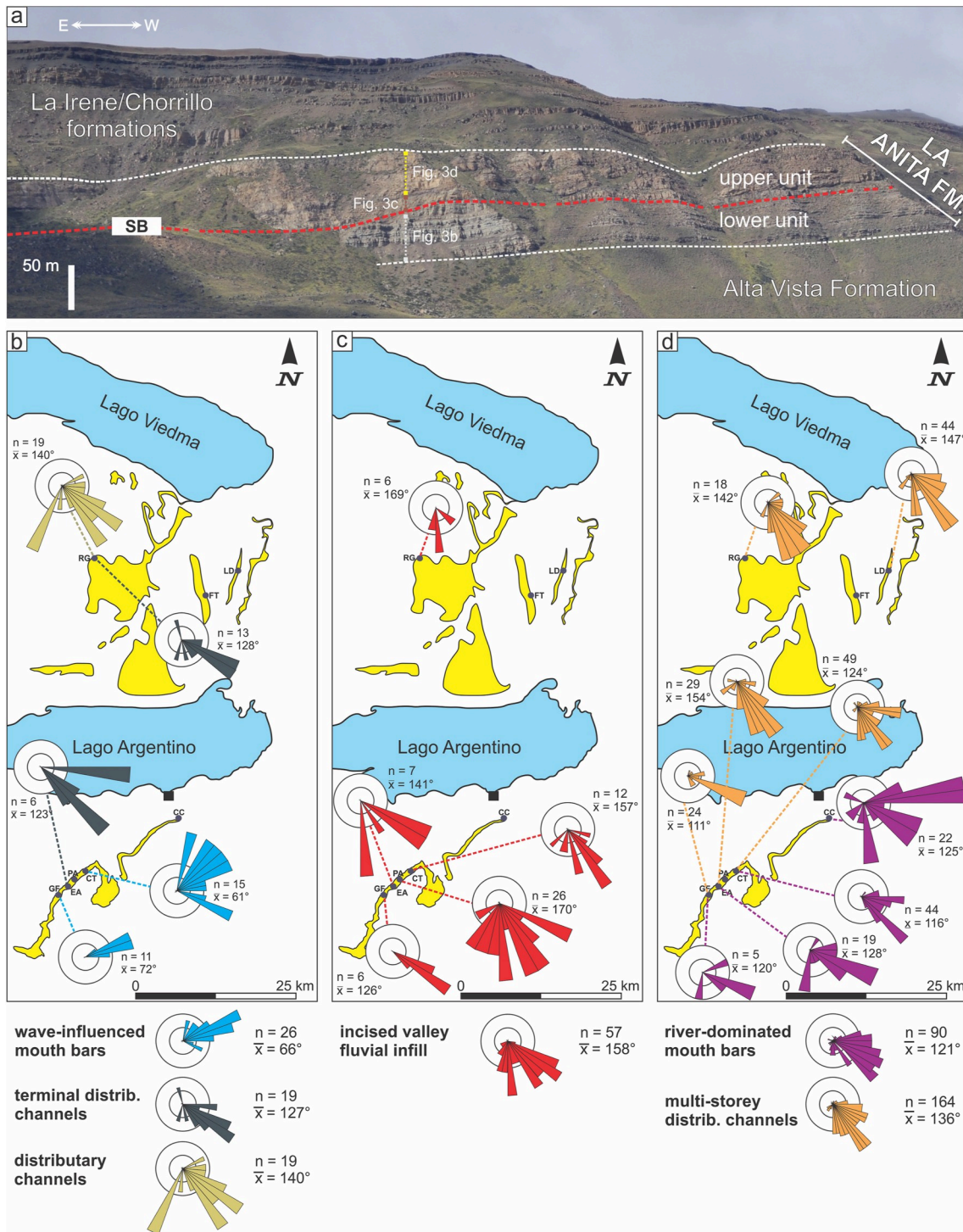
Fig. 3. a) Outcrop panel showing the stratigraphic position of the La Anita Formation, the division of the two informal units bounded by the sequence boundary (SB) and the position of the paleoenvironments where paleocurrent directions where measured. Geological maps showing the LAF exposures and paleocurrent rose diagrams for the: b) wave-dominated, river-influenced deposits of the lower unit, c) incised valley fluvial infill of the lowermost interval of the upper unit, and d) river-dominated, tidal-influenced delta of the upper unit.

Net and Limarino, 2000).

Cements are represented by hematite, silica and carbonate which behave as pore lining, pore filling, grain coating and sometimes replacing detrital grains reducing the pore space. Different diagenetic processes and products were also identified with conventional petrography and were described in the Diagenesis section (*see* section 7.1).

5.1. Detrital components

Monocrystalline quartz: this component is the most abundant crystal clast type of the LAF with abundance values ranging between 13% and 23%, with an average of 19%. This component shows typical characteristics of volcanic origin such as straight extinction, commonly with embayments, partial presence of crystalline faces and surfaces free of inclusions. These grains are subrounded to subangular (Fig. 5a).
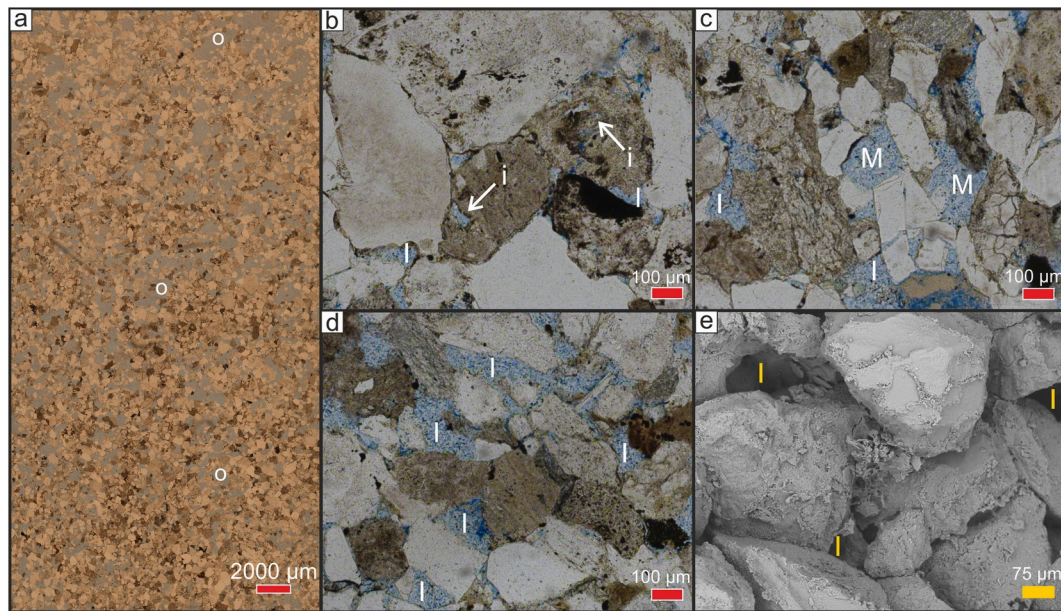
Fig. 4. Photomicrographs showing pore textures. a) General view of the slide section showing pore abundance and oversized texture (o); b) Intragranular (i) and intergranular (I) pore textures; c) Intergranular (I) and moldic (M) pore textures; d) Intergranular pore texture (I); e) Intergranular pore texture (I) under SEM.

Potassium feldspar: the abundance of these grains ranges between 3% and 9%, with an average of 6%. These are the most abundant feldspar type and are subrounded to subangular. The dominant type is the orthoclase (Fig. 5b), and in lower proportions microcline is present (Fig. 5c).

Plagioclase: this component is less abundant than K-feldspars, ranging between 1% and 4%, with an average of 3%. These gains are typically subangular and they are twinned according to the albite law (Fig. 5d).

Polycrystalline quartz: these grains are scarce, their abundance ranges between 2% and 12% (7% on average). These grains are composed of individual crystals larger than 62 μm which are mainly anhedral, elongate-shaped and have undulating extinction and saturated boundaries (Fig. 5e). This component corresponds to the coarse-grained type of polycrystalline quartz (*sensu* Limarino and Giordano, 2016) which suggests a metamorphic origin.

Volcanic lithic: these are the most common detrital component of the LAF (25–50%, 42% on average). The grains are subrounded and can be divided into two types according to their textures. Some of these volcanic rock fragments are characterized by pilotaxitic texture, which is recognized by small, chaotically distributed, euhedral to subhedral, plagioclase crystals, in an aphanitic groundmass. Pilotaxitic texture is characteristic of the intermediate volcanic groundmass. Other volcanic lithics present an internal felsitic texture which consists of an aphanitic texture, crypto to microcrystalline, formed by an association of small equidimensional feldspar and quartz crystals (Fig. 5f).

Sedimentary lithic (Ls): this type of rock fragment abundance ranges between 0% and 2%. Most consist of mudstone and siltstone intraclasts (Fig. 5g), uncommonly there are fine-grained sandstones. They are rounded, internally structureless and uncommonly presented as part of the pseudomatrix.

Phytodetritus (Pd): these correspond to terrestrial organic matter particles which abundance ranges between 0.25% and 8%. These grains are presented in two types: a pale brown in color variant that preserves some features of its original vegetable texture indicating low decomposition degree (Fig. 5h). Other grains are dark brown in color and do not preserve original vegetable textures indicating a higher degree of decomposition (Fig. 5h).

5.2. Sandstone classification

The LAF sandstones are composed of rock fragments (66%), monocrystalline quartz (23%) and feldspars (11%). Detrital modes were plotted in Folk et al. (1970) and Dott (1964) modified by Pettijohn et al. (1972) ternary diagrams.

All the analyzed sandstones are classified as litharenites according to the Folk et al. (1970) classification (Fig. 6a). Considering the diagram proposed by Dott (1964), modified by Pettijohn et al. (1972), which discriminates not only detrital components but also by the matrix abundance, the sandstones of the LAF are classified as lithic arenites (Fig. 6b).

5.3. Provenance

Detrital modes were plotted in traditional sandstones provenance ternary graphs (Dickinson and Suczek, 1979; Dickinson et al., 1983; Dickinson, 1988) and are shown in Fig. 6. Although the efficiency of these diagrams is discussed (Ingersoll, 1990; Ingersoll et al., 1993; Critelli and Ingersoll, 1995), many authors accept and use them (e.g., Suczek and Ingersoll, 1985; Packer and Ingersoll, 1986). Moreover, there are many provenance studies of the AMB that use them (Manassero, 1988; Macellari et al., 1989; Romans et al., 2011; Varela et al., 2013; Richiano et al., 2015; Malkowski et al., 2017; Sickmann et al., 2019).

When locating the samples of the LAF in the ternary diagrams, a low data dispersion can be observed. In the QtFL diagram of Dickinson et al. (1983), the analyzed sandstones are grouped in the limit of the recycled orogen and transitional arc areas (Fig. 6c). Regarding the proportion of monocrystalline quartz in the QmFLt, the analyzed samples show higher affinity to the recycled orogenic field of the Dickinson et al. (1983) diagram (Fig. 6d), and in the recycled orogen sand suites area of the Dickinson (1988) diagram (Fig. 6e). In these last, a certain affinity with the transitional arc and volcaniclastic sand fields is maintained for some samples from the upper unit of the LAF (Fig. d and e).

The diagram of Dickinson and Suczek (1979) for sandstones with a high proportion of lithic fragments was used in order to differentiate those samples coming from the orogen from the ones related to the magmatic arc. In this, it is highlighted that the sandstones of the LAF are located within the magmatic arc field (Fig. 6f).
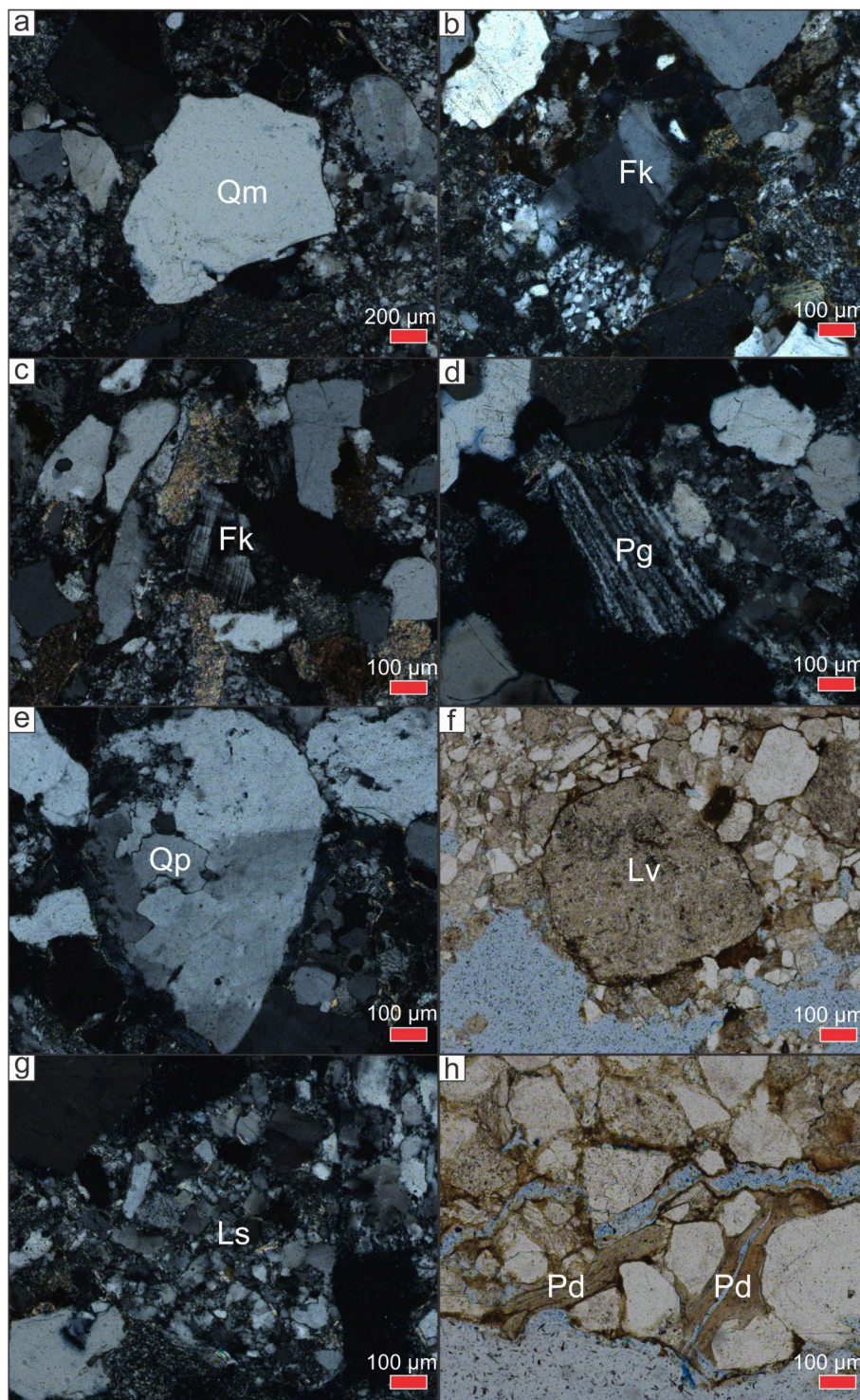
Fig. 5. Detrital component. a) Monocrystalline quartz (Qm); b) Potassium feldspar (Fk), orthoclase which is twinned according to the Carlsbad law; c) Potassium feldspar (Fk): microcline displaying typical lattice twinning; d) Plagioclase (Pg) twinned according to the albite law; e) Polycrystalline quartz (Qp); f) Volcanic lithic (Lv); g) Sedimentary lithic (Ls); h) Phytodetritus (Pd).

6. X-RAY diffraction (XRD)

From the whole-rock XRD analysis variable proportions of quartz, potassium feldspar, plagioclase, calcite, dolomite and clay minerals were recognized (Table 2; Fig. 7). Quartz is the dominant mineral in most of the analyzed samples, its content is abundant to very abundant. Plagioclase and potassium feldspar contents are very scarce to scarce. Calcite and dolomite are present as scarce minerals and are not present

in all the samples, their values are less than 5%, but exceptional calcite values have been recorded reaching 45% for specific samples of the lower unit in CT locality, associated with the presence of bioclastic sandstones. Clay minerals are present in variable proportions, they are very scarce to abundant with higher contents in the fine-grained samples, where they increase to the detriment of quartz.

Clay fraction analysis indicates that the LAF is characterized by a variable proportion of illite, chlorite, kaolinite, and smectite as well as
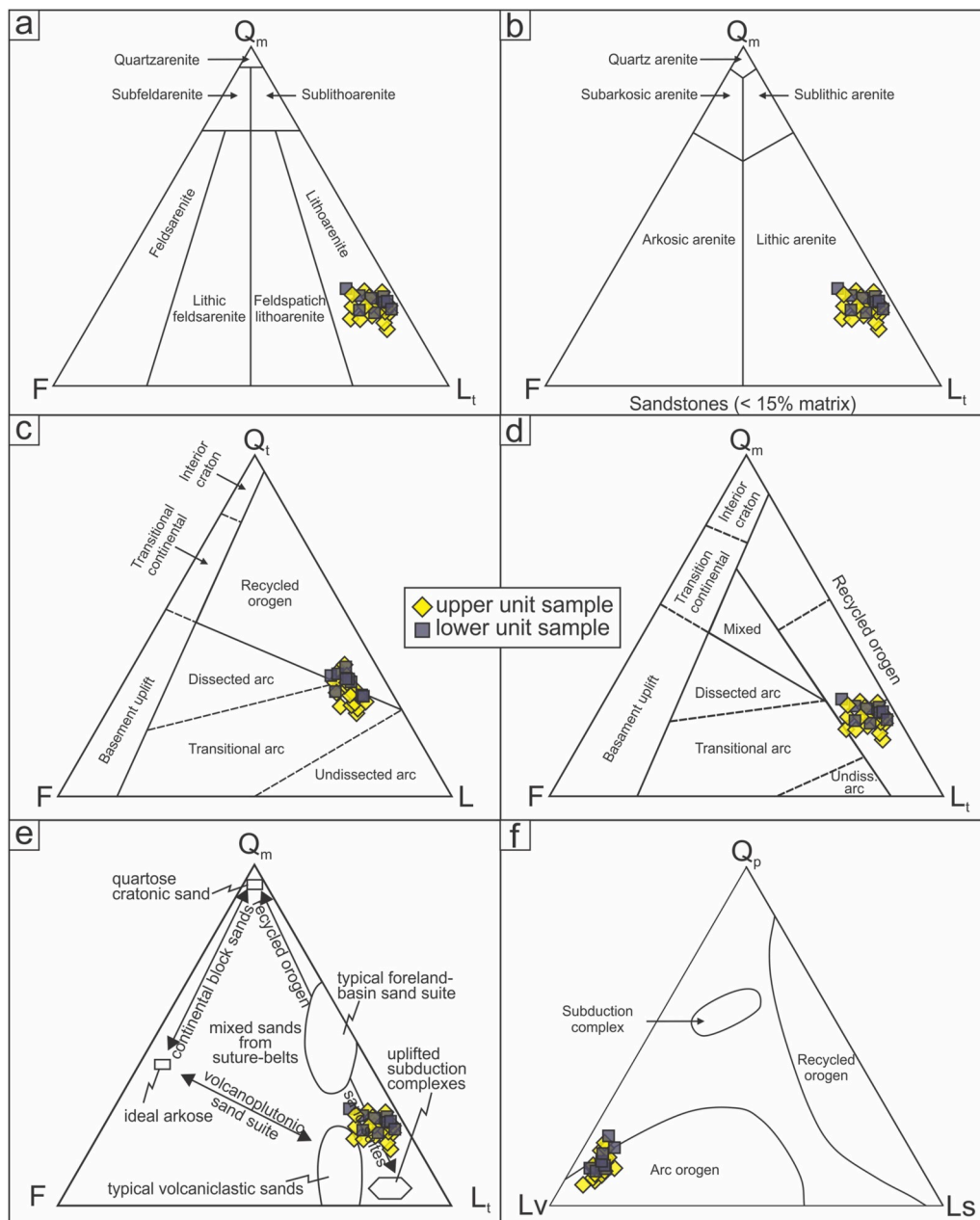
Fig. 6. Classification and provenance of LAF sandstones. a) Folk et al. (1970); b) Dott (1964), modified by Pettijohn et al. (1972), c) Dickinson et al. (1983); d) Dickinson et al. (1983); e) Dickinson (1988); f) Dickinson and Suczek (1979).

interstratified minerals including illite-smectite and chlorite-smectite (Table 2; Fig. 8). Illite is scarce to moderate in RG, CC, CT and moderate to abundant in GF and EA with maximum values documented in fine-grained samples. It is characterized on oriented aggregates by their (00l) reflections at 9.94, 4.98 and 3.33 Å (Fig. 9a and b). These peaks show no changes on air-dried, ethylene-glycol saturation and heating to 550 °C samples, and according to the sharp and symmetrical form of the illite ~10 Å peak, a high crystallinity is considered (Eberl and Velde, 1989). Chlorite is not present in all the samples, but when it does, is very scarce to moderate as observed in some samples from RG, CC, CT, GF and EA. The basal reflections at ~ 14.30, 7.03 and 3.53 Å (Fig. 9a, c) are observed, however in many samples from CT, GF and EA there is a shift in ethylene-glycol solvated patterns towards lower angles which suggest the presence of some expandable layers within the structure of chlorite. Kaolinite is recognized by diagnostic peaks at 7.15, and 3.58 Å ranging from scarce to very abundant as documented through the analyzed

locations (Fig. 9b, d). This mineral represents an important phase in deposits of the LAF, in particular, kaolinite dominates in the lower unit at GF, many sandstone levels at EA, and in sandstones of the upper unit at CC. The content of this mineral decreases considerably in fine-grained intervals where enrichment of illite, smectite and/or illite-smectite is observed in both the lower and upper units. Smectite is not present in all the analyzed samples, but when it does, is scarce to abundant and characterized on XRD oriented ethylene-glycol solvated patterns by a broad peak at 17.0 Å (Fig. 9b), with a low resolution of its low-angle side. In most samples, illite-smectite (I/S) interstratified minerals are present with moderate to very abundant contents as recorded in sandstones of the lower unit at RG, sandstones of the upper unit at CT, and many fine-grained samples in conjunction with smectite (Fig. 9a, c). According to the positions of 001(I)/002(S) and 002(I)/003(S) of ethylene-glycol solvated patterns, I/S is characterized by random to partially ordered types (R0 to R1) with a relative abundance of illite
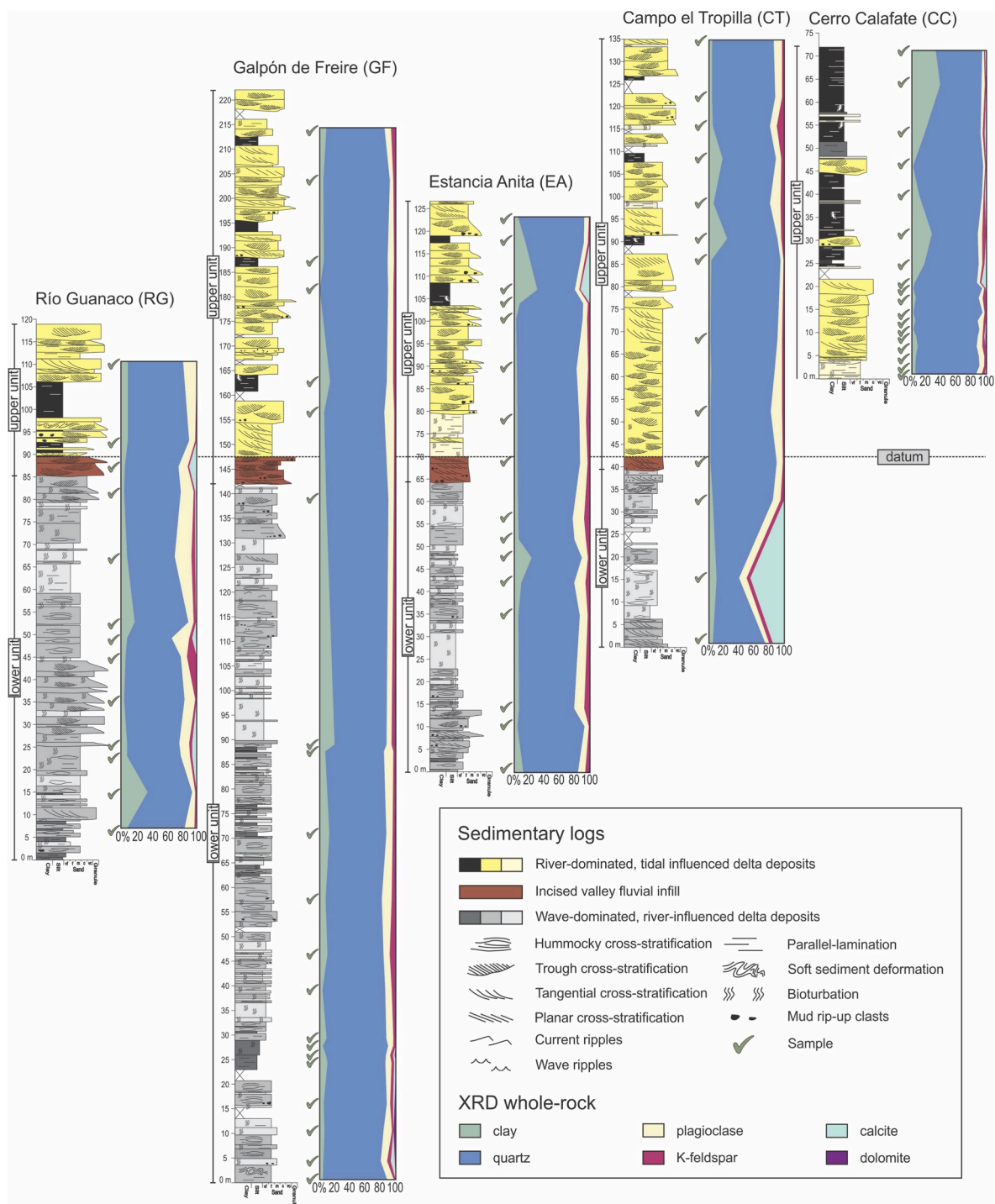
Fig. 7. Results of the whole-rock composition based on X-ray diffraction patterns of the LAF.

layers in the order of 40–60% (Moore and Reynolds, 1997).

7. Diagenesis

An integrated approach between conventional sandstone petrography and SEM enables the identification of diagenetic processes and products. Also, SEM analysis in sandstone samples made possible the corroboration of cross-cutting relationships between different diagenetic products in addition to examining the origin of clay minerals.

7.1. Diagenetic products and processes

Diagenetic processes and their associated products identified in the petrographic and SEM studied samples are listed below in relatively chronological order. Not all the diagenetic products were found in all samples.

Compaction: different compaction products were recognized in the studied sedimentary sections. Mechanical compaction is evidenced by different types of grain contacts, microfractures and pseudomatrix. Long and concave-convex contacts are abundant between detrital grains while sutured contacts are infrequent (Fig. 10a). Transgranular and
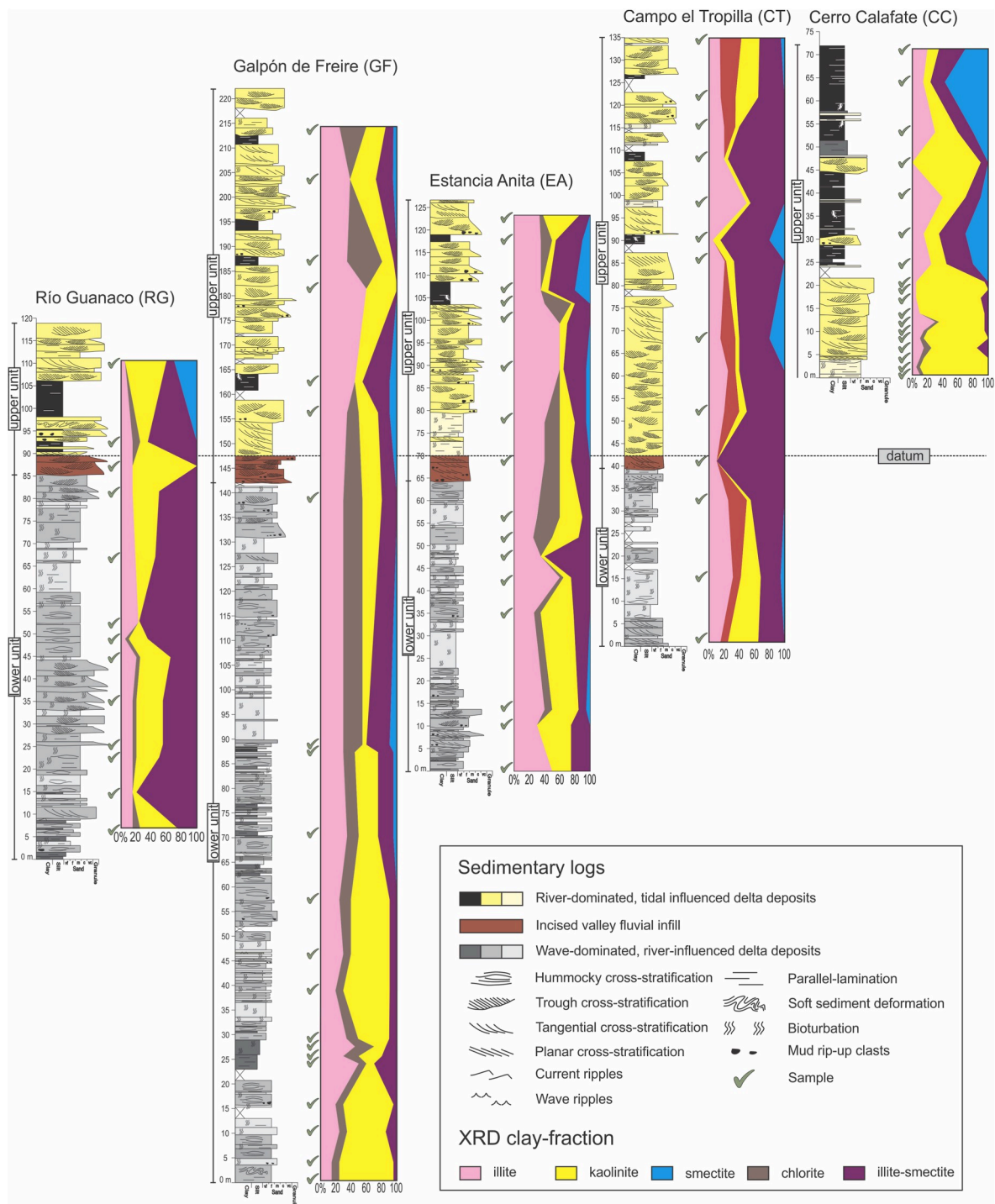
Fig. 8. Results of the clay-fraction based on X-ray diffraction patterns of the LAF.

intragranular microfractures are common in all studied samples (Fig. 10b and c). Pseudomatrix is scarce and was recognized only in the GF section (Fig. 10d). Chemical compaction is evidenced by simple microstylolites with organic matter presence and was identified only in the CT locality (Fig. 10e).

Dissolution: this process was recognized only in the GF section and is evidenced through the porosity in some selected grains of potassium feldspars, intraclasts, volcanic lithics, and eventual skeletal grains. Intragranular porosity is common and oversized, while moldic porosity is rare (Fig. 10f). The pore size is mainly micropore (less than 0.62 μm) and connectivity between them could not be recognized.

Clay replacement: this process is common and was recognized in all the analyzed samples and consists in the partial to total alteration of volcanic lithic and feldspars grains by authigenic clay minerals (Fig. 10g and h), mainly kaolinite. Kaolinite occurs mainly as booklets that consist of thin (1–3 μm thick) pseudohexagonal crystals (Fig. 11a). These were recognized also as infill of voids left by the dissolution of detrital grains (Fig. 11b). In addition, volcanic lithics are replaced partially by chlorite (Fig. 11c).

Hematite cementation: this type of cement was identified as affecting the entire sample or as patches (Fig. 11d and e). Hematite minerals behave as pore lining, pore filling, grain coating and sometimes
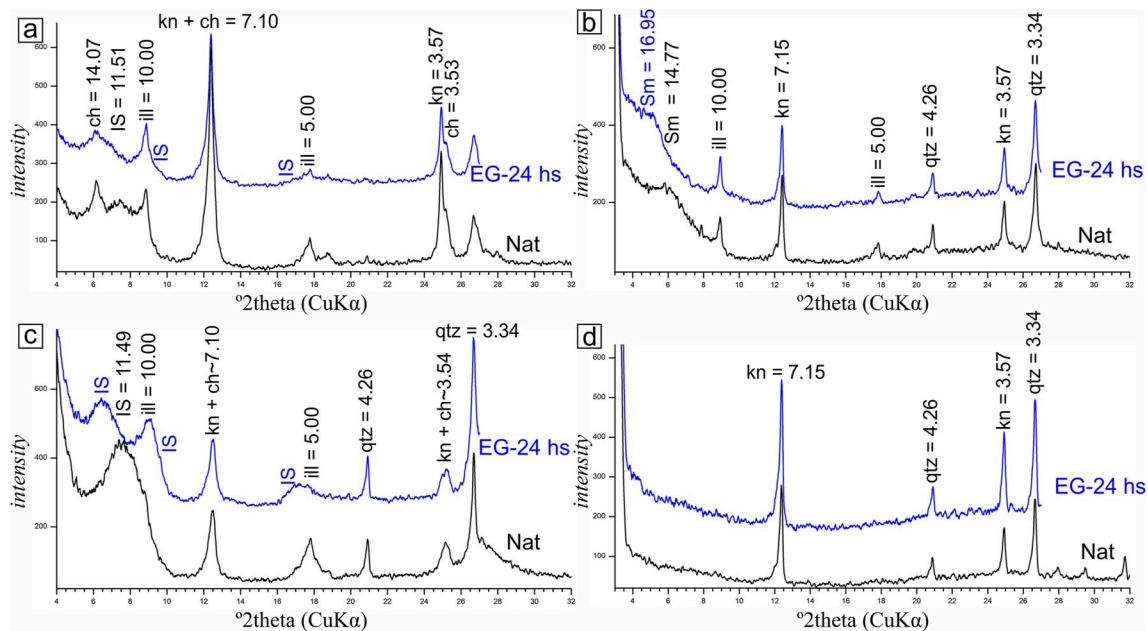
Fig. 9. Examples of representative X-ray diffractograms of the clay-fraction of LAF showing the position of peaks expressed in Angstroms. a) sample CT 159 with chlorite, illite, kaolinite and illite/smectite mixed layers; b) sample CC Ca 50 with the contribution of illite, kaolinite, and smectite; c) sample CT 128 dominated by illite/smectite mixed layers and a minor proportion of illite and kaolinite; d) sample RG-101 dominated by kaolinite. References: Qtz (quartz), Ill (illite), Sm (smectite), IS (illite/smectite mixed layers), Kn (kaolinite), and Ch (chlorite).

replacing detrital grains. Although it is present in isolated samples of all the study sedimentary sections, it develops especially towards the top of the CT locality. In the samples with hematite cementation, most of the clay minerals and detrital grains look stained by iron oxide, thus they show reddish stain color.

Clay authigenesis: this process was recognized in all the analyzed samples and is represented by clay coatings. These coatings are less than 10 μm thick and are formed by smectite (and illite-smectite inter-stratified minerals) occurring on the surface of framework grains, except at points of grain-to-grain contact (Fig. 11f). Smectite displayed a typical honeycomb texture characteristic of authigenic products (Fig. 11g and h). Clay crystals are usually enveloped by quartz overgrowths.

Silica cementation: silica cement is present in all the studied localities and typically occurs as thin overgrowths on detrital quartz grains. The width of most overgrowths is less than 20 μm thick (Fig. 12a and b) and has optical and crystallographic continuity with detrital quartz grains.

Carbonate cementation: carbonate cement includes only calcite in patches in isolated samples of CC and GF localities (Fig. 12c). Calcite crystals are inequigranular, their size ranges between 20 and 800 μm and fills pore spaces between detrital grains.

Bitumen migration: bitumen is present in all sedimentary sections as grain coating, pore lining (Fig. 12d), pore filling and fracture filling (Fig. 12e). The textural relationships indicate that the deposition of the solid bitumen post-dates the carbonate cementation.

Pyritization: this process is present in all the studied localities and is represented by the presence of isolated or framboidal in shape, sub-hedral to euhedral, pyrite crystals up to 15 μm in size (Fig. 12f).

7.2. Paragenetic sequence

Through an integrated approach with conventional sandstone petrography and SEM, a diagenetic history is proposed for the LAF (Fig. 13). A detailed description of the paragenetic sequence is developed below.

During the early stages of diagenesis, compaction of sand grains involved closer packing and mechanical reorganization of the

components. The lithostatic pressure caused fracturing of brittle grains and bending of weak grains. The concave-convex sutured contacts (Fig. 10a) and deformed muscovite and phytodetritus (Fig. 10d) indicated that sandstones were compacted due to lithostatic pressure during early diagenesis (Yasin and Ibrahim, 2017; Abbasi and Yasin, 2017). The lithostatic pressure and water mineral interaction caused the partial or total dissolution of volcanic lithic and feldspar and transformation in authigenic clay minerals such as kaolinite and chlorite as was documented under SEM and optical microscopy (Fig. 10g and h and 11a-c).

The diagenesis continues with a clay coating and silica cement (Fig. 13). Both processes reduce pore and throat spaces. The dissolution of feldspar and unstable minerals of lithic (volcanic) fragments can result in authigenic kaolinite (Xu et al., 2003; Zhang et al., 2009), which also conforms dense aggregates filling cavities (intergranular pores) between detrital grains (Fig. 11a and b). The smectite (and illite-smectite interstratified minerals) overlain detrital quartz forming clay coating (Fig. 11g and h). Illite-smectite typically begins to form during mesodiagenesis at temperatures that exceed about 70 °C (Worden and Morad, 2003). The persistence of smectite besides illite-smectite with high amounts of expandable layers suggests that deep burial conditions (temperature >110 °C) were not reached. The silica cement post-dated the clay coating and is represented by thin quartz over-growths (Fig. 12a and b). The potential source of silica for quartz cementation could be internal (i.e., related to the quartz grains) because it is volumetrically insignificant (Worden and Morad, 2000). However more precise studies as oxygen isotope are needed to confirm this origin (Hyodo et al., 2014). Different authors proposed the diagenetic transformation of clays from smectite precursors to illite via illite-smectite interstratified minerals as a source of quartz cement in other sandstone deposits of the AMB (e.g., Spalletti et al., 2005; Richiano et al., 2015).

The advanced stage of diagenesis is related to calcite cementation, a new phase of compaction and bitumen migration (Fig. 13). The quartz overgrowth is succeeded by calcite, which was then partially fractured, and secondary pores and microfractures were filled with bitumen. Carbonate cement includes calcite crystals in patches filling pore spaces between detrital grains (Fig. 12c). The source of calcite could be related
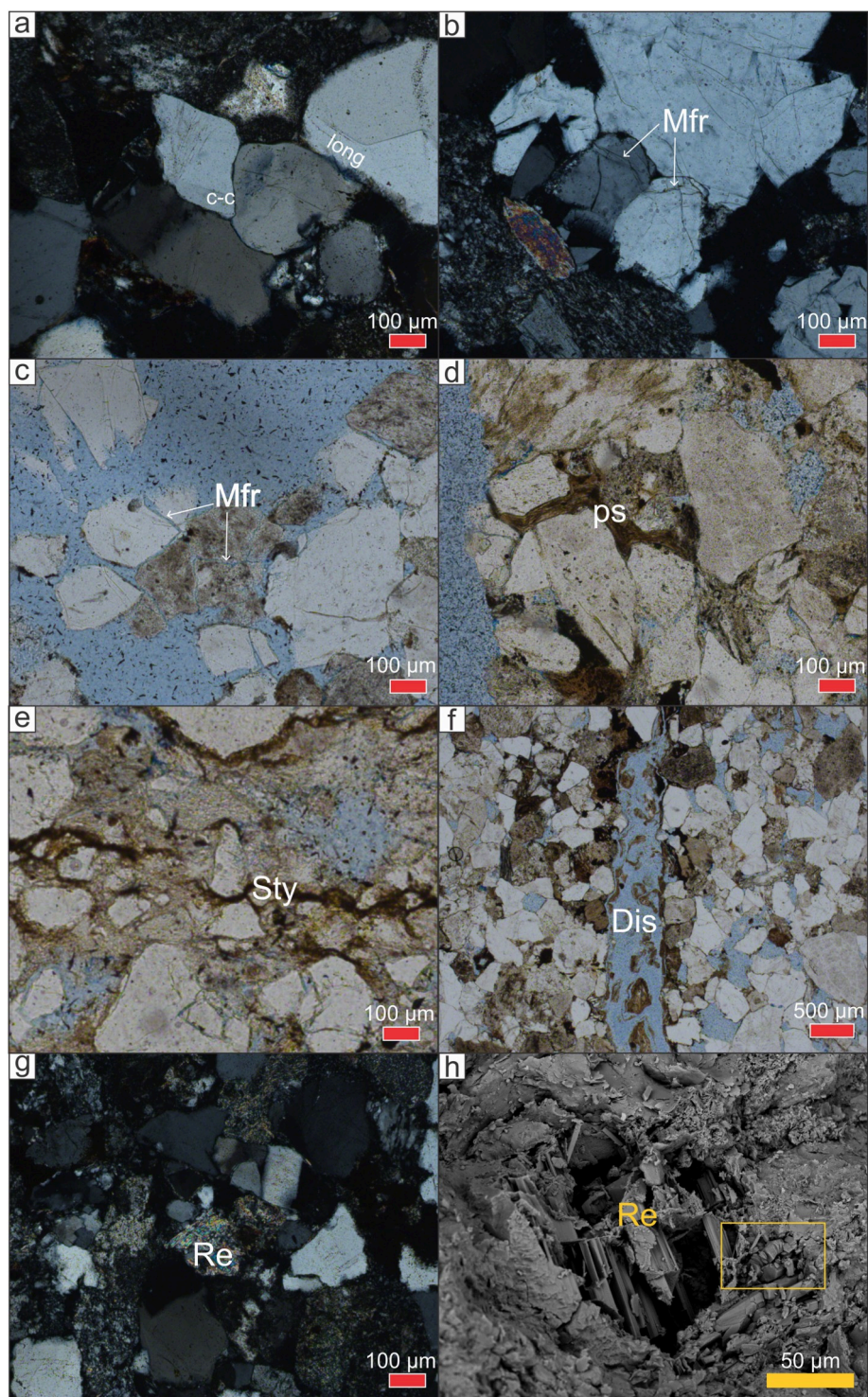
Fig. 10. Photomicrographs showing diagenetic processes and products. a) Compaction: long and concave-convex contacts; b) Compaction: closed fractures (Mfr, white arrows); c) Compaction: open transgranular fractures (Mfr, white arrows); d) Compaction: pseudomatrix (ps); e) Compaction: microstylolites (Sty); f) Dissolution: moldic porosity (Dis); g) Clay replacement: partially replacement of volcanic lithic (Re); h) Clay replacement: partially replacement of potassium feldspars (Re).

to the dissolution of skeletal grains (Fig. 10f). The second phase of compaction is represented by the presence of transgranular and intra-granular microfractures (Fig. 10b and c). This process is interpreted as post-dated calcite cement through cross-cutting relationships. Bitumen (Fig. 12f) fills pore spaces and microfractures and coats authigenic kaolinite or quartz overgrowth. Organic geochemistry, fluid inclusion and biomarkers studies are needed to know the origin of bitumen, but the textural relationships indicate that the migration phase post-dates the second compaction phase.

Hematite cement (Fig. 11d and e) is present in some samples of the LAF upper unit filling pore spaces, coating grains and altering some detrital grains. This cement postdated the second phase of compaction but its cross-cutting relation with bitumen migration could not be recognized. Detrital Fe–Mg silicate grains could be a local source of Fe
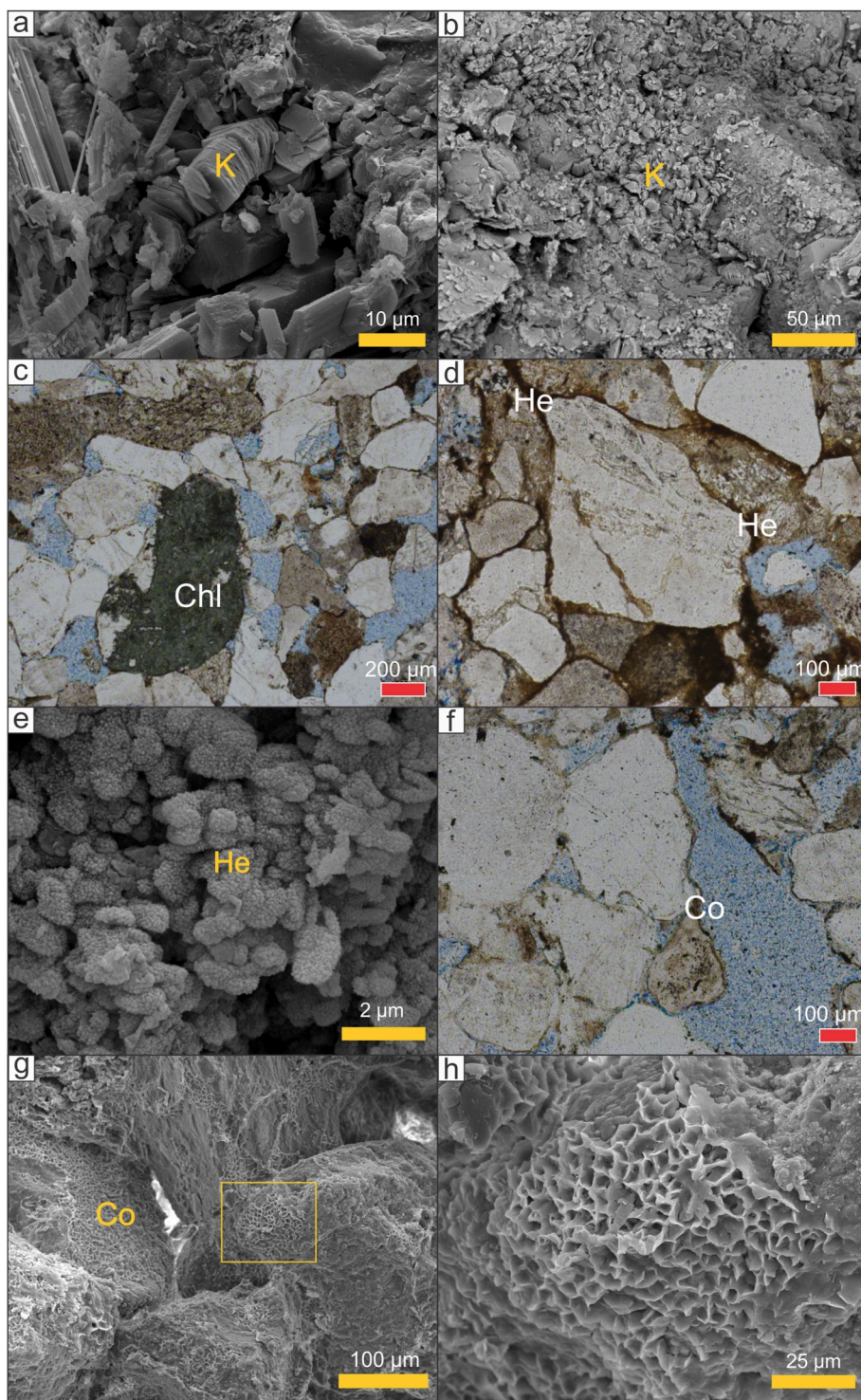
Fig. 11. Photomicrographs showing diagenetic processes and products. a) Clay replacement: partially replacement of potassium feldspars by kaolinite (k) in pseudohexagonal crystals (detail of Fig. 10h); b) Clay replacement: kaolinite (k) crystals infill voids left by the dissolution of detrital grains; c) Clay replacement: volcanic lithics replaced partially for chlorite (chl); d) Hematite cementation: a patch of hematite cementation (he); e) Hematite cementation: hematite crystals (he); f) Clay authigenesis: clay coatings (Co); g) Clay authigenesis: Smectite coating (Co); h) Clay authigenesis: Smectite coating with typical honeycomb texture (Co, detail of Fig. 11g).

for some authigenic hematite (Lu et al., 1994), although a large amount of this cement suggests that an external source is also required.

Pyritization of organic matter is the last process in diagenetic history. Pyrite (Fig. 12f) is recognized over detrital grains and cements. The precipitation of pyrite could be related to the degradation of the abundant organic matter present in the sediment that would generate local reducing conditions (Berner, 1984).

8. Discussion

8.1. Controls on the composition of the La Anita formation

The composition of the LAF has been analyzed by conventional petrography, XRD and SEM, in order to detect the compositional variability of these deposits. From the sandstone petrographic analysis, it is highlighted that all the samples are classified as lithic arenites with low matrix content (Fig. 6a and b). No significant differences in detrital modes or vertical trend can be observed between the analyzed samples
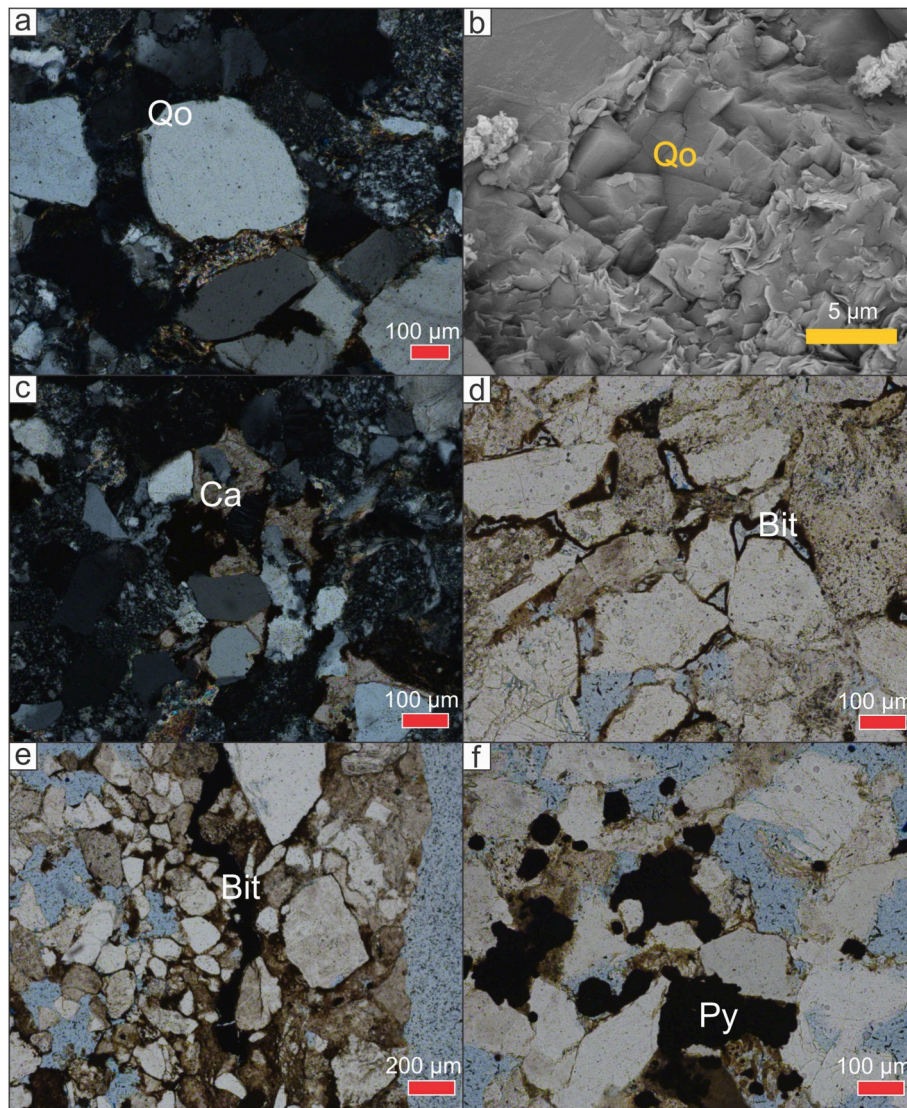
Fig. 12. Photomicrographs showing diagenetic processes and products. a) Silica cementation: quartz overgrowths (Qo); b) Silica cementation: detail of quartz overgrowths (Qo); c) Carbonate cementation: Calcite crystals (Ca) fill the pore spaces between detrital grains; d) Bitumen migration: bitumen as pore-filling (Bit); e) Bitumen migration: bitumen as fracture filling (Bit); f) Pyritization: framboidal pyrite (Py).
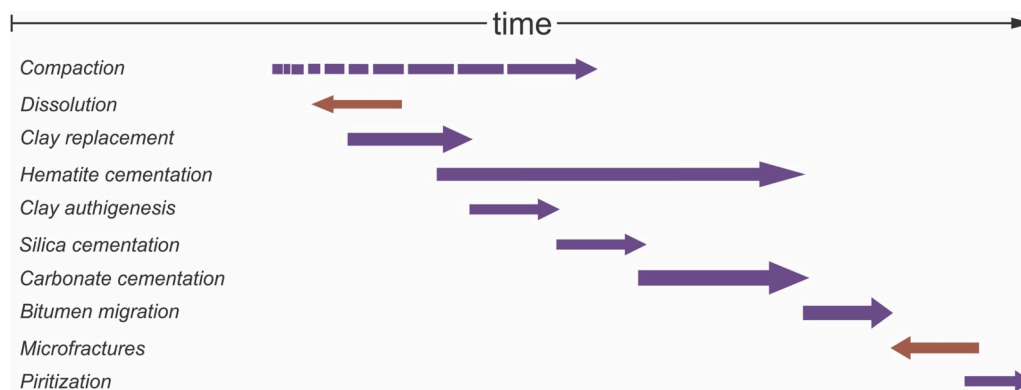
Fig. 13. Diagenetic sequence of sandstone of LAF. Blue arrows represent processes that increase the porosity and red arrows represent processes that decrease the porosity. The width of the arrow represents the magnitude of the process. (For interpretation of the references to color in this figure legend, the reader is referred to the Web version of this article.)

of the lower unit with respect to the upper unit, reflecting a homogeneous detrital composition. Whole-rock XRD analyses also show a relatively homogeneous composition throughout the entire unit (Fig. 7). On the other hand, the clay-fraction reflects that the LAF is characterized by variable proportions of illite, kaolinite, smectite and mixed-layer illite-smectite with the sporadic presence of chlorite. Although there are no significant changes in the clay-fraction composition, kaolinite tends to dominate in sandstones of the lower unit with an increase in the abundance of smectite and illite-smectite clay-minerals towards the upper unit (Fig. 8).

The detrital and authigenic composition of sedimentary successions is controlled by different factors. Tectonic processes generate elevated areas that act as sediment sources and also control the rates of sediments supply (Dickinson et al., 1983; Zattin et al., 2003; Cavazza and Ingersoll, 2005; Stefani et al., 2007). Climate influences the rate of sediment available for transport but also impacts the authigenesis of clay-minerals (Galán, 2006; Raigemborn et al., 2014). Chemical weathering processes prevail under tropical humid climates and control the composition of siliciclastic sediments (Nesbitt and Young, 1982; Middelburg et al., 1988; Raigemborn et al., 2014; Wanas and Assal, 2021). By contrast, physical weathering dominates under arid climates and includes the fragmentation of source rock into smaller grain sizes without significant changes in chemical or mineralogical composition (Nesbitt and Young, 1982). Depositional environments may also influence the composition of sediment due to local controls such as carbonate production and pedogenesis processes, among others (e.g., Lundegard, 1994; Morad et al., 2010; Varela et al., 2013, 2018). During sediment burying, diagenetic processes may enhance and affect the original composition of the deposits via diagenetic alterations and cement precipitations as well as preserve or destroy porosity and permeability (Morad et al., 2010). A brief discussion of each one of these compositional controls will be developed in the next pages.

8.1.1. Tectonic influence on sandstone provenance

Foreland basins receive detrital material mainly from three different sources: i) the volcanic arc, ii) the fold-thrust belt, and iii) the stable craton and the uplifted continental blocks on the periphery of the basin (Nie et al., 2012). The AMB foreland system received detrital material from these three main sediment source areas (Varela et al., 2013; Richiano et al., 2015; Malkowski et al., 2017; Sickmann et al., 2019; Odino et al., 2021; Ghiglione et al., 2021).

The magmatic arc, associated with the west compressive margin of South America, began to develop during the Late Cretaceous in the western sector of the basin (Ramos et al., 1982; Bruce et al., 1991; Hervé et al., 2007; Varela et al., 2013). The development and evolution of the fold-thrust belt toward the west of the basin uplifted the Paleozoic metasedimentary complexes known as the Eastern Andean Metamorphic Complex and the Jurassic rocks of the El Quemado Complex (157-145 Ma) which is mainly composed of acidic volcanic and volcaniclastic rocks associated to the synrift stage of the basin (Pankhurst et al., 2000; Ghiglione et al., 2021). Peripheral areas that supplied sediment correspond to the older Chon Aike volcanic (200-157 Ma) which are represented in the Deseado and North Patagonian Massifs (Pankhurst et al., 2000; Varela et al., 2013; Malkowski et al., 2017; Sickmann et al., 2019).

The use of the conventional sandstone provenance ternary diagrams is based on the fact that they use components that are present in all the stratigraphic units of the study area and because several published studies of other units of the basin use them. In some cases, provenance ternary diagram is followed by U–Pb detrital zircon provenance analysis that gives sustenance to the interpretations (Fildani and Hessler, 2005; Romans et al., 2011; Varela et al., 2013; Richiano et al., 2015; Cereceda, 2016; Malkowski et al., 2017; Sickmann et al., 2019; Ghiglione et al., 2021).

Sample plots on different used ternary diagrams are homogeneous, showing low data dispersion, and no difference is recognized in the provenance of the samples analyzed from the lower unit with those from

the upper unit of the LAF (Fig. 6). Provenance from recycled orogen would imply that these sediments are part of a secondary depositional cycle that reworked the components of an orogen. In this way, it is proposed that these sandstones have mixed features with affinity both for the magmatic arc and for a recycled orogen raised by the fold-thrust belt. Considering that, (1) the basin deepens to the south, and (2) the paleoflow measurements the LAF indicate a southeast progradation direction both for the lower and upper unit (Fig. 3; Moyano-Paz et al., 2018), suggesting that the sediment source areas were located toward the west/northwest.

The obtained plots show certain similarities with previous studies published for underlying and overlying formations and also contemporary stratigraphic units of the basin (Fig. 14a; Romans et al., 2011; Varela et al., 2013; Cereceda, 2016; Malkowski et al., 2017; Sickmann et al., 2019). Recently, Sickmann et al. (2019) presented a detailed study differentiating the provenance of detrital zircons for different stratigraphic intervals of the AMB. The discrimination did for the Tres Pasos (Alta Vista)/Dorotea (La Anita) stratigraphic interval also suggests a provenance from a magmatic arc and a fold-thrust belt as the analyzed samples for the LAF (Fig. 14b). Although the development of the fold-thrust belt affected both the Paleozoic Eastern Andean Metamorphic Complex and the El Quemado Complex, the scarce proportion of metamorphic components, which are practically restricted to polycrystalline quartz and detrital illite, indicate that the supply of these sources was mainly from uplifted areas of the El Quemado Complex (Fig. 14c).

Climate and environmental influence on clay minerals composition.

Clay minerals present in sedimentary successions can be detrital or authigenic in origin (Chamley, 1989). Detrital clay minerals are those that come from an external source and that have been almost none modified during transport. By contrast, authigenic clay-minerals are those neoformed or transformed in situ (Wilson and Pittman, 1977).

The origin of smectite and kaolinite clay minerals was determined by morphological observations under SEM images and by the shape of their diagnostic peaks observed in the clay-fraction diffractograms (Figs. 9b and 11g and h). Kaolinite occurs mainly as booklets that consist of thin (1–3 μm thick) pseudohexagonal crystals, and smectite displays a typical honeycomb texture characteristic of an authigenic origin. Moreover, both kaolinite and smectite show well-formed peaks suggesting good crystallinity and therefore supporting an authigenic origin in the depositional environment. Illitic clay could not be detected under SEM and was only determined by XRD (Fig. 9a, b and c). A detrital origin is proposed for illite clay mineral considering that the Paleozoic Eastern Andean Metamorphic Complex, which is characterized mainly by illite, chlorite and white micas (Hervé et al., 2008), acted as source area.

Smectite clay minerals can be formed as the product of the alternation of volcanic or volcaniclastic components due to authigenic processes under diverse climatic conditions (Chamley, 1989; Galán, 2006; Raigemborn et al., 2014). Otherwise, kaolinite may be formed as chemical weathering (lixiviation) of precursor minerals such as smectite, mica, feldspar, and volcanic and volcaniclastic components under warm and humid tropical conditions (Senkayi et al., 1987; Chamley, 1989; Marfil et al., 2003; Galán, 2006; Raigemborn et al., 2014). In this way, the same volcanic material under warm and humid climatic conditions could form kaolinite as the main clay minerals, while in temperate climatic conditions smectite should be the expected dominant clay-mineral (Chamley, 1989; Thiry, 2000; Raigemborn et al., 2014).

The increment of authigenic smectite in detriment of authigenic kaolinite recorded in the LAF could reflect a change in the paleoclimatic conditions in the depositional area, or at least in the rainfall regime. Although several works stand that for the Upper Cretaceous the climate was dominantly warm and humid and with no major fluctuations of global scale unlike the Lower and early Upper Cretaceous (Jenkyns, 1980; Barron et al., 1989; Föllmi, 2012; Friedrich et al., 2012; Robinson et al., 2017; O'Brien et al., 2017; O'Connor et al., 2019). The presence of authigenic kaolinite and the scarce to null participation of authigenic
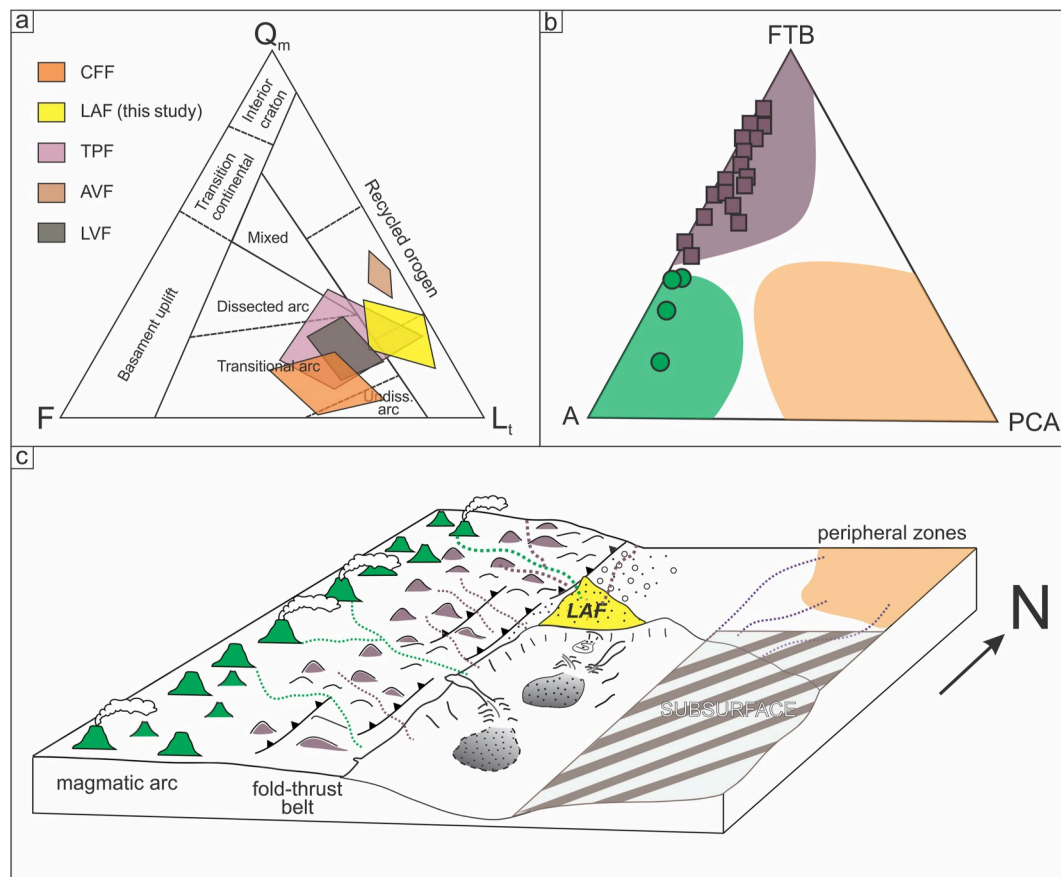
Fig. 14. a) Comparison with the obtained sandstone provenance results with previous provenance studies. LVF = Lago Viedma Formation (Malkowski et al., 2017), AVF = Formación Alta Vista (Cereceda, 2016); TPF = Tres Pasos Formation (Romans et al., 2011; Sickmann et al., 2019); LAF = La Anita Formation; CFF = Cerro Fortaleza Formation (Varela et al., 2013). b) Detrital zircon provenance diagram (modified from Sickmann et al., 2019), FTB = fold thrust belt; A = arc; PCA = peripheric Chon Aike. c) Scheme of the sources that supplied detrital material to the LAF.

smectite in the lower unit deposits could indicate a high rate of chemical weathering under tropical climates with high rainfall (Thiry, 2000; Raigemborn et al., 2014) and this is consistent with the role of depositional processes which show a strong influence of storm events (Moyano-Paz et al., 2018, 2020). On the contrary, the increment of authigenic smectite in detriment to the authigenic kaolinite observed for the upper unit could be related to the formation of smectite in the fine-grained poorly drained water-logged soils of the interdistributary areas (Moyano-Paz et al., 2018) under more temperate seasonal climatic conditions (Raigemborn et al., 2014). The presence of authigenic smectite clay minerals formed by alteration of volcanic components coming from the Late Cretaceous magmatic arc is the result of pedogenesis under temperate seasonal climatic conditions (Varela et al., 2013, 2018). These seasonal climatic conditions could also explain the episodic sedimentation of turbidity or density currents in the river-dominated distal delta front associated with fluctuations in the fluvial discharges (Moyano-Paz et al., 2020).

8.1.2. Diagenetic influence on the composition

The link between detrital composition and diagenetic products is especially interesting because the detrital composition is very homogeneous but diagenetic history is slightly different in the LAF deposits. Comparing the lower unit with respect to the upper unit, no significant differences in detrital modes or vertical trend can be observed (Figs. 6 and 7). Clay-fraction has no significant vertical changes but an increment in the abundance of smectite clay minerals is observed, from the lower to the upper unit, to the detriment of kaolinite (Fig. 8). On the other hand, the diagenetic products are different in both units. In the

lower unit, we identified scarce carbonate cement and thick quartz overgrowth. Conversely, in the upper unit, we recognize abundant carbonate cement (preferably in the CC section), hematite cement (CT section) and pseudomatrix (GF section) that are not present in the lower unit.

The difference in the behavior between composition and diagenetic products can be explained through the depositional facies which in turn may control the composition of pore fluids. While the lower unit is interpreted as accumulated in a storm wave-dominated, river-influenced deltaic depositional system, the upper unit was mainly accumulated by a river-dominated, tidal influenced deltaic depositional system (Moyano-Paz et al., 2018, 2020). In wave-dominated deltas like the one of the lower unit of the LAF, the riverine freshwater is easily diluted by the wave action and pore water composition is mainly marine. In these cases, sandstone deposits that are poor in carbonate grains have lower potential to develop eogenetic carbonate cementation and maintain relatively high intergranular porosities (Morad et al., 2000). During mesodiagenesis, quartzose sandstones may become extensively cemented by quartz overgrowths if grain coatings are not well developed (Bloch et al., 2002).

In river-dominated deltas, like the one recorded in the upper unit of the LAF, sandstone deposits display patterns of diagenetic alterations, including the formation of carbonate cement (especially calcite), pseudomatrix formation, hematite cement and thin authigenic coatings of smectite clay (Moraes and Surdam, 1993; Lundegard, 1994). The carbonate cementation is usually associated with layers rich in carbonate bioclasts or mud intraclasts along flooding surfaces (Morad et al., 2010). The formation of pseudomatrix is due to the mechanical compaction of

mud intraclasts eroded from floodplain deposits. In delta-front deposits developed in warm, tropical, river-dominated deltas is common the presence of grain coating and Fe-rich clays. Such settings promote the formation of these clays due to high sedimentation rates, abundant iron-bearing particles from rivers, and brackish pore-water compositions (Johnsson, 1990; Kronen and Glenn, 2000). Brackish pore waters have lower concentrations of dissolved sulfate ions than marine pore waters. Thus, less $Fe+2$ is sequestered in pyrite, making more of it available for Fe-rich clays formation (Odin, 1985, 1990) and for hematite cement during mesodiagenesis. Other eogenetic alterations in deltaic sandstone related to tidal influence include the formation of grain-coating smectite, which is transformed into illite via illite-smectite interstratified minerals during mesodiagenesis (Morad et al., 2010).

8.2. Impact of diagenesis on primary porosity values and reservoir properties

Conventional sandstone reservoirs are often shown to be controlled by facies types and spatial distribution of facies (Fic and Pedersen, 2013; Shanmugam, 2012). However, post-depositional diagenetic processes may affect reservoir primary depositional features, enhancing, preserving, or destroying primary porosity and permeability and therefore affecting the reservoir properties (Morad et al., 2010; Higgs et al., 2013; Henares et al., 2016). In the LAF sandstones, diagenetic processes affect primary porosity values by increasing them or reducing them in different magnitudes.

Carbonate and hematite cementation are diagenetic processes that significantly reduce pore volume (Dapples, 1971; Lu et al., 1994; Zhang et al., 2009). In the LAF sandstones, calcite crystals fill the spaces between detrital grains (Fig. 12c) and significantly reduce the porosity to values between 2 and 10%, depending on the size of the patch. Hematite minerals are presented as pore lining, pore filling, grain coating and sometimes replacing detrital grains (Fig. 11d and e), this process reduces the porosity to values between 1 and 10%, depending also on the size of the patch. Both processes are more frequent in the upper unit of the LAF. While calcite cement is present in samples of CC and GF localities, hematite cement develops especially towards the top of the CT locality.

Other diagenetic processes identified in the LAF reduce the porosity but not significantly, such as early mechanical compaction phase, clay coating and replacement, silica cement and bitumen migration. The early mechanical compaction phase is represented by long and concave-convex grain contacts (Fig. 10a) in all the studied sections. The small proportion of sutured contacts and pseudomatrix in addition to the abundance of ductile lithic grains (mainly volcanic lithic; Figs. 5 and 6) evidence low reduction of porosity probably related to textural parameters (grain size fine to very fine-grained sandstone) or low burial depth (<2 km; Bjørlykke, 1999). During early diagenesis, volcanic lithics and potassium feldspars grains are replaced partially or completely for clay minerals, mainly kaolinite and chlorite (Fig. 10g and h and 11a and c). Although these clay minerals were recognized also as infill voids left by the dissolution of detrital grains (Fig. 11b), the magnitude of this diagenetic process is not enough to generate a significant reduction in poral space. Clay coating was recognized in all the samples as <10 μm thick smectite coatings (Fig. 11f–h). Grain-coating smectitic clays could be an important factor in the evolution of reservoir quality and heterogeneity because the formation of smectite coating could inhibit quartz cementation preserving the primary porosity (Al-Ramadan and El-Khoriby, 2013). Silica cement typically occurs as overgrowths on detrital quartz grains (Fig. 12a and b). The quartz overgrowths do not significantly reduce porosity due to their thinness (<20 μm thick), probably related to previous development of clay rims (Morad et al., 2010). Bitumen is present in all the studied localities as grain coating, pore lining, pore filling and fracture filling (Fig. 12d and e), but it only accumulates significantly in two samples of CT locality. Solid bitumen occurs in carbonate and siliciclastics petroleum reservoirs in many basins worldwide (e.g., Jones and Speers, 1976; Wilhelms and Larter,

1995; Horstad and Larter, 1997; Huc et al., 2000), and forms barriers in the reservoirs, which prevents economic petroleum production (Shalaby et al., 2012).

Post-depositional dissolution and late mechanical compaction phase, where microfracture generates, increase porosity values. These kinds of pores are denominated as secondary porosity (Taylor et al., 2010). In the LAF deposits, secondary porosity is represented mainly as intragranular, oversized and moldic pore types. The petrographic evidence suggests that these pores are related to the dissolution of potassium feldspars, intraclasts and volcanic lithics grains (Fig. 10f). Regarding the microfractures, which are the less frequent secondary pore type observed in the LAF, these are generally closed and occasionally open (Fig. 10b and c) without non-associated mineralization, although in some cases a few fractures are filled by solid bitumen. The volume of secondary porosity is <1%, which coincides with some authors who suggest the contribution of dissolution to porosity is commonly volumetrically minor (<2%; Taylor et al., 2010; Bjørlykke, 2014).

The porosity of the LAF sandstones is mainly primary with moderate to good abundance and micropore to mesopore as main pore-sizes (Fig. 4). The porosity is highly variable throughout the localities mainly due to diagenetic calcite and hematite cementation presence (Fig. 15). These kinds of cements are more frequent in the upper unit of the LAF which is interpreted as the fluvial infill of an incised valley (Fig. 15), and then as a river-dominated, tide-influenced deltaic depositional system in the uppermost interval (Fig. 15c; Moyano-Paz et al., 2018, 2020). Contrary, the lower unit of the LAF which is interpreted as a wave-dominated, river-influenced delta (Moyano-Paz et al., 2018, 2020), has a lower potential to develop carbonate and hematite cementation and maintain relatively high intergranular porosities (Fig. 15; Morad et al., 2010). Thus, the principal control affecting the porosity is the diagenetic processes, these are in turn controlled by the depositional facies (Fig. 15).

Natural siliciclastic reservoirs are commonly classified as either conventional reservoirs or tight reservoirs (e.g., Zou et al., 2012; Moore et al., 2016). They differ in several properties including depositional conditions, diagenetic history, pore type and origin, pore throat structures and permeability (Zhao et al., 2007; Zou et al., 2012). The LAF has been defined and exploited as a tight type of reservoir in some sectors of the AMB (Jait et al., 2018). Tight sandstone reservoirs are characterized by a composition dominated by feldspar crystal clasts, reaching mid to late diagenetic stages, low porosity values (<12%), the dominance of secondary porosity, low permeability (≤0.1) and a high fluid saturation (45–70%), among other characteristics (e.g., Surdam et al., 1997; Holditch, 2006; Zou et al., 2010, 2012). Although LAF sandstones have similar porosity values to tight reservoirs (13% in the lower unit and 8.5% in the upper unit), the pore origin and the general composition is more like those of conventional reservoirs. The studied sandstones are composed mainly of volcanic lithic grains and monocrystalline quartz while feldspar crystals are always in smaller proportion (<10%; Table 1). Also, secondary porosity (Fig. 4) is considerably low (<2%) as exposed before and does not contribute significantly to the general abundance. Although detailed fluid saturation and permeability are needed to have a complete picture of the reservoir properties and characteristics of the LAF, it has good potential characteristics to develop as a conventional reservoir analog from wave- and river-dominated deltas.

9. Conclusions

● The detrital and authigenic composition of the LAF is controlled by tectonic processes, climate influences, depositional conditions and diagenetic processes. The sandstones of the LAF are all classified as lithic arenites with low matrix content and show a homogeneous detrital composition.
● The source that supplied detrital material was the magmatic arc developed during the Late Cretaceous and the recycled orogen raised
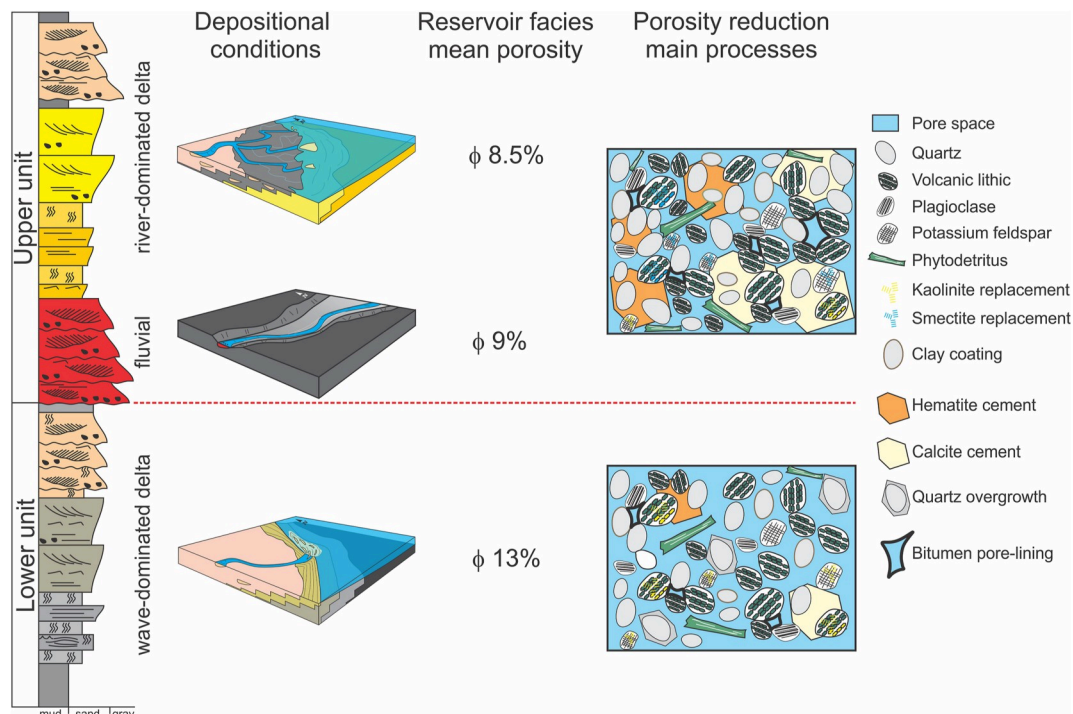
Fig. 15. Schematic sedimentary section of the LAF showing facies distribution, depositional conditions, mean porosity values, and processes reducing the porosity of the wave-dominated and river-dominated reservoir units.

by the fold-thrust belt associated mainly with the El Quemado Complex. These source areas were located toward the west/north-west of the accumulation zone.

- The origin of smectite and kaolinite clay mineral was determined as authigenic by morphological observations at SEM and by the shape of diagnostic peaks observed in the clay-fraction diffractograms.
- A change in the paleoclimatic conditions, or at least in the rainfall regime, can be highlighted by the vertical variation of authigenic clay minerals from the lower to the upper unit evolving from tropical climates with high rainfall and a high rate of chemical weathering where kaolinite dominates, to more temperate seasonal climatic conditions where smectite formed in poorly drained paleosols.
- The diagenetic processes are controlled especially by the depositional facies type which also control the fluid pore composition. In the wave-dominated lower unit scarce carbonate cement and thick quartz overgrowth occur. Conversely, in the river-dominated upper unit carbonate and hematite cementation is frequent, and pseudo-matrix is recognized.
- The principal control over the porosity and reservoir properties are the diagenetic processes, which are in turn controlled by the type and distribution of facies. Carbonate and hematite cementation are diagenetic processes that significantly reduce pore volume. Other diagenetic processes identified in the LAF reduce the porosity but not significantly, such as mechanical compaction, clay coating and replacement, silica cement and bitumen migration. Depositional dissolution and fracture processes increase the porosity, but the volume of this is considerably low (<1%).
- The porosity of the LAF sandstones is mainly primary with moderate to good abundance and micropore to mesopore as the main pore-sizes. The porosity is highly variable throughout the localities mainly due to diagenetic calcite and hematite cementation presence. These kinds of cement are more frequent in the upper unit than the lower unit.

Declaration of competing interest

The authors declare that they have no known competing financial interests or personal relationships that could have appeared to influence the work reported in this paper.

References

Abbasi, N., Yasin, M., 2017. Petrography and diagenetic history of Nagri formation sandstone in district Bagh and Muzaffarabad. Pakistan: Pak. J. Geriatr. 1, 21–23.

Al-Ramadan, K., El-Khoriby, E., 2013. Integrated diagenesis and sequence stratigraphic study of tidal sandstones: the Adedia Formation (Cambro-Ordovician), Sinai, Egypt. Arabian J. Geosci. 6 (6), 2009–2020.

Barron, E.J., Hay, W.W., Thompson, S., 1989. The hydrologic cycle. A major variable during Earth history. Palaeogeogr. Palaeoclimatol. Palaeoecol. 75, 157–174.

Berner, R.A., 1984. Sedimentary pyrite formation: an update. Geochem. Cosmochim. Acta 48, 605–615.

Bianchi, J.L., 1967. Informe preliminar acerca de los perfiles estratigráficos realizados en el sector Occidental de la Cuenca Austral, durante las campañas 1964-65 y 1965- 66. Unpublished report, Yacimientros Petrolíferos Fiscales (Y.P.F.).

Biddle, K., Uliana, M., Mitchum Jr., R., Fitzgerald, M., Wright, R., 1986. The stratigraphic and structural evolution of central and eastern Magallanes Basin, Southern America. In: Allen, P.A., Homewood, P. (Eds.), Foreland Basins, vol. 8. International Association of Sedimentologist Special Publication, pp. 41–61.

Biscaye, P.E., 1965. Mineralogy and Sedimentation of Recent Deep-Sea Clay in the Atlantic Ocean and Adjacent Seas and Oceans, vol. 76. Geological Society of America Bulletin, pp. 803–832.

Bjørlykke, K., 1999. An Overview of Factors Controlling Rates of Compaction, Fluid Generation and Flow in Sedimentary Basins. In: Jamtveit, B., Meakin, P. (Eds.), Growth, Dissolution and Pattern Formation in Geosystems. Springer, Dordrecht. https://doi.org/10.1007/978-94-015-9179-9_18.

Bjørlykke, K., 2014. Relationships between depositional environments, burial history and rock properties. Some principal aspects of diagenetic process in sedimentary basins. Sediment. Geol. 301, 1–14.

Bloch, S., Lander, R.H., Bonell, L., 2002. Anomalously High Porosity and Permeability in Deeply Buried Sandstone Reservoirs: Origin and Predictability, vol. 86. American Association of Petroleum Geologists, Bulletin, pp. 301–328.

Bossi, G.E., 2007. Análisis de Paleocorrientes: San Miguel de Tucumán. Ediciones Magna, p. 200.

Brindley, G.W., 1961. In: Methods, Experimental, Brown, G. (Eds.), The X-Ray Identification and Crystal Structure of Clay Minerals. Mineralogical Society, pp. 1–50.

Brown, G., 1980. Tables for the determination of d in Å from 2θ for the Kα and Kβ radiations of cooper, cobalt and iron. In: Brindley, G.W., Brown, G. (Eds.), Crystal Structures of Clay Minerals and Their X-Ray Identification: Mineralogical Society Monograph 5, pp. 439–475.

Bruce, R.M., Nelson, E.P., Weaver, S.G., Lux, D.R., 1991. Temporal and spatial variations in the southern Patagonian batholith: constraints on magmatic arc development. In: Harmon, R.S., Rapela, C.W. (Eds.), Andean Magmatism and its Tectonic Setting, vol. 265. Geological Society of America Special Paper, pp. 1–12.

Cavazza, W., Ingersoll, R.V., 2005. Detrital modes of the ionian Forearc basin fill (Oligocene-Quaternary) reflect the tectonic evolution of the Calabria-Peloritani Terrane (southern Italy). J. Sediment. Res. 15, 268–279.

Cereceda, A., 2016. Sedimentología de los depósitos marinos de las formaciones Cerro Toro y Alta Vista, Cretácico Superior, Cuenca Austral [PhD Thesis]. Universidad Nacional de La Plata, La Plata, p. 271.

Chamley, H., 1989. Clay Sedimentology. Springer, Berlin, p. 623.

Critelli, S., Ingersoll, R.V., 1995. Interpretation of neovolcanic versus paleovolcanic sand grains: an example from Miocene deep marine sandstones of the Topanga Group (Southern California). Sedimentology 42, 783–804.

Daniels, B.G., Auchter, N.C., Hubbard, S.M., Romans, B.W., Matthews, W.A., Stright, L., 2018. Timing of deep-water slope evolution constrained by large-n detrital and volcanic ash zircon geochronology. Cretaceous Magallanes Basin, Chile: Geological Society of America Bulletin 130, 438–454.

Daniels, B.G., Hubbard, S.M., Romans, B.W., Malkowski, M.A., Matthews, W.A., Bernhardt, A., Kaempfe, S.A., Jobe, Z.R., Fosdick, J.C., Schwartz, T.M., Fildani, A., Graham, S.A., 2019. Revised chronostratigraphic framework for the Cretaceous Magallanes-Austral basin, Última Esperanza Province, Chile. J. S. Am. Earth Sci. 94, 102209.

Dapples, E.C., 1971. Physical classification of carbonate cement in quartzose sandstones. J. Sediment. Petrol. 41, 196–204.

DeCelles, P.G., Langford, R.P., Schwartz, R.K., 1983. Two new methods of paleocurrent determination from trough cross-stratification. J. Sediment. Petrol. 53, 629–642.

Dickinson, W.R., 1970. Interpreting detrital modes of graywake and arkose. J. Sediment. Petrol. 40, 695–707.

Dickinson, W.R., 1988. Provenance and Sediment Dispersal in Relation to Paleotectonics and Paleogeography of Sedimentary Basins. New Perspectives in Basin Analysis. Springer, Nueva York, pp. 3–25.

Dickinson, W.R., Rich, E.I., 1972. Petrologic Intervals and Petrofacies in the Great Valley Sequence, Sacramento Valley, California, vol. 83. Geological Society of America Bulletin, pp. 3007–3024.

Dickinson, W.R., Suczek, C., 1979. Plate Tectonics and Sandstone Composition, vol. 63. American Association of Petroleum Geologists Bulletin, pp. 2164–2182.

Dickinson, W.R., Beard, L.S., Brakenridge, G.R., Erjavec, J.L., Ferguson, R.C., Inman, K. F., Knepp, R.A., Lindberg, F.A., Ryberg, P.T., 1983. Provenance of North American Phanerozoic Sandstones in Relation to Tectonic Setting, vol. 94. Geological Society of America Bulletin, pp. 222–235.

Do Campo, M., Del Papa, C., Nieto, F., Hongn, F., Petrinovic, I., 2010. Integrated analysis for constraining palaeoclimatic and volcanic influences on clay-mineral assemblages in orogenic basins (Palaeogene Andean foreland, North-western Argentina). Sediment. Geol. 228, 98–112.

Dott, R.H., 1964. Wacke, greywacke and matrix-what approach to immature sandstone classification? J. Sediment. Petrol. 34, 625–632.

Eberl, D.D., Velde, B., 1989. Beyond the Kubler index. Clay Miner. 24 (3), 571–577.

Fic, J., Pedersen, P.K., 2013. Reservoir characterization of a "tight"oil reservoir, the middle Jurassic upper Shaunavon member in the Whitemud and Eastbrook pools, SW Saskatchewan. Mar. Petrol. Geol. 44, 41–59.

Fildani, A., Hessler, A., 2005. Stratigraphic Record across a Retroarc Basin Inversion: Rocas Verdes-Magallanes Basin, Patagonian Andes, Chile, vol. 117. Geological Society of America Bulletin, pp. 1596–1614.

Folk, R.L., Andrews, P.B., Lewis, D.W., 1970. Detrital sedimentary rock classification and nomenclature for use in New Zealand. N. Z. J. Geol. Geophys. 13, 937–968.

Föllmi, K.B., 2012. Early Cretaceous life, climate and anoxia. Cretac. Res. 35, 230–257.

Fosdick, J.C., Romans, B.W., Fildani, A., Bernhardt, A., Calderon, M., Graham, S.A., 2011. Kinematic Evolution of the Patagonian Retroarc Fold-And-Thrust Belt and Magallanes Foreland Basin, Chile and Argentina, 51°30'S, vol. 123. Geological Society of America Bulletin, pp. 679–698.

Friedrich, O., Norris, R.D., Erbacher, J., 2012. Evolution of middle to Late Cretaceous oceans - a 55 m. y. record of Earth's temperature and carbon cycle: Geology 40 (2), 107–110.

Galán, E., 2006. Genesis of clay minerals. In: Berhaya, F., Theng, B.K.G., Lagaly, G. (Eds.), Handbook of Clay Science, Developments in Clay Science. Elsevier, The Netherlands, pp. 1129–1162.

Gazzi, P., 1966. Le arenarie del flysch sopra cretaceo dell'Appennino modenese: correlazioni con il flysch di Monghidoro. Mineral. Petrogr. Acta 16, 69–97.

Ghiglione, M.C., Naipauer, M., Sue, C., Barberón, V., Valencia, V., Aguirre-Urreta, B., Ramos, V.A., 2015. U-Pb zircon ages from the northern Austral basin Patagonia. Cretac. Res. 55, 116–128.

Ghiglione, M.C., Rocha, E., Raggio, M.F., Ramos, M.E., Ronda, G., Moyano-Paz, D., Varela, A.N., Valencia, V., 2021. Santonian-Campanian continentalization in the Austral-Magallanes basin: regional correlation, provenance and geodynamic setting. Cretac. Res. 128, 104968.

Gómez-Peral, L.E., Raigemborn, M.S., Poire, D.G., 2011. Petrología y evolución diagenética de las facies silicoclásticas del Grupo Sierras Bayas, Sistema de Tandilia, Argentina. Lat. Am. J. Sedimentol. Basin Anal. 18, 3–41.

Henares, S., Caracciolo, L., Viseras, C., Fernández, J., Yeste, L.M., 2016. Diagenetic constraints on heterogeneous reservoir quality assessment: a Triassic outcrop analog of meandering fluvial reservoirs. AAPG (Am. Assoc. Pet. Geol.) Bull. 100 (9), 1377–1398.

Hervé, F., Pankhurst, R.J., Fanning, C.M., Calderón, M., Yaxley, G.M., 2007. The South Patagonian batholith: 150 m.y. of granite magmatism on a plate margin. Lithos 97 (3–4), 373–394.

Hervé, F., Calderón, M., Faúndez, V., 2008. The metamorphic complexes of the Patagonian and Fuegian Andes. Geol. Acta: Int. Earth Sci. J. 6 (1), 43–53.

Higgs, K.E., Funnell, R.H., Reyes, A.G., 2013. Changes in reservoir heterogeneity and quality as a response to high partial pressures of CO2 in a gas reservoir. New Zeland: Matine Petrol. Geol. 48, 293–322.

Holditch, S.A., 2006. Tight gas sands. J. Petrol. Technol. 58 (6), 86–93.

Horstad, I., Larter, S.R., 1997. Petroleum migration, alteration, and remigration within Troll field, Norwegian north sea. American Assoc. Petrol. Geol. 81 (2), 222–248.

Hubbard, S.M., Fildani, A., Romans, B.W., Covault, J.A., Mchargue, T.R., 2010. High relief slope clinoform development: insights from outcrop, Magallanes Basin, Chile. J. Sediment. Res. 80, 357–375.

Huc, A.Y., Nederlof, P., Debarre, R., Capentier, B., Boussafir, M., Laggoun-DÉfarge, Lenail-Chouteau, A., Bardas Le Floch, N., 2000. Pyrobitumen occurrence and formation in a Cambro-ordovician sandstone reservoir, Fahud Salt basin. North Oman Chem. Geol. 168, 99–112.

Hyodo, A., Kozdon, R., Pollington, A.D., Valley, J.W., 2014. Evolution of quartz cementation and burial history of the Eau Clair Formation based on insitu oxygen isotope of quartz overgrowths. Chem. Geol. 384, 168–180.

Ingersoll, R.V., 1983. Petrofacies and Provenance of Late Mesozoic Forearc Basin, Northern and Central California, vol. 67. American Association of Petroleum Geologists Bulletin, pp. 1125–1142.

Ingersoll, R.V., 1990. Actualistic sandstone petrofacies: discriminating modern and ancient source rocks. Geology 18, 733–736.

Ingersoll, R.V., Bullard, T.F., Ford, R.L., Grimm, J.P., Pickle, J.D., Sares, S.W., 1984. The effect of grain size on detrital modes: a test of the Gazzi-Dickinson point-counting method. J. Sediment. Res. 54 (1), 103–116.

Ingersoll, R.V., Kretchmer, A.G., Valles, P.K., 1993. The effect of sampling scale on actualistic sandstone petrofacies. Sedimentology 40, 937–953.

Jait, D.M., Cevallos, M., Molinari, M.L., Cangini, A., Mas Cattapan, F., Vega, V., 2018. Exploración y desarrollo de reservorios de baja permeabilidad de la formación Magallanes en el bloque El Cerrito, Cuenca Austral, Argentina: 10° Congreso de Exploración y Desarrollo de Hidrocarburos Simposio de Desarrollo de Hidrocarburos. Desarrollo con pensamiento No Convencional, Mendoza, pp. 235–251.

Jenkyns, H.C., 1980. Cretaceous anoxic events: from continents to oceans. J. Geol. Soc. 137, 171–188.

Johnsson, M.J., 1990. Tectonics versus chemical-weathering controls on the composition of fluvial sands in tropical environments. Sedimentology 37, 713–726.

Jones, H.P., Speers, R.G., 1976. Permo-triassic reservoirs of Prudhoe Bay field. In: North Slope, Alaska, vol. 24. American Asociation of Petroleum Geologists Memoir, p. 23.

Kronen Jr., J.D., Glenn, C.R., 2000. Pristine to reworked verdine: keys to sequence stratigraphy in mixed carbonate-siliciclastic fore reef sediments (Great Barrier Reef). In: Glenn, C.R., Prevot-Lucas, L., Lucas, J. (Eds.), Marine Authigenesis: from Global to Microbial, vol. 66. SEPM Special Publication, pp. 387–403.

Lai, J., Wang, G., Wang, S., Cao, J., Li, M., Pang, X., Zhou, Z., Fan, X., Dai, Q., Yang, L., He, Qin, Z., 2018. Review of diagenetic facies in tight sandstones: diagenesis, diagenetic minerals, and prediction via well logs. Earth Sci. Rev. 185, 234–258.

Limarino, C.O., Giordano, S.R., 2016. Unraveling multiple provenance areas using sandstone petrofacies and geochemistry: an example in the southern flank of the Golfo San Jorge Basin (Patagonia, Argentina). J. S. Am. Earth Sci. 66, 208–231.

Lu, G., Mccabe, C., Henry, D.J., Schedl, A., 1994. Origin of hematite carrying a late Paleozoic remagnetization in a quartz sandstone bed from the Silurian rose hill formation. Virginia, USA Earth Planet Sci. Lett. 126, 235–246.

Lundegard, P.D., 1994. Mixing zone origin of 13C-depleted calcite cement: oseberg Formation sandstones (Middle Jurassic), Veslefrikk field, Norway. Geochem. Cosmochim. Acta 58, 2661–2675.

Macellari, C.E., Barrio, C.A., Manassero, M.J., 1989. Upper Cretaceous to Paleocene depositional sequences and sandstone petrography of southwestern Patagonia (Argentina and Chile). J. S. Am. Earth Sci. 2, 233–239.

Malkowski, M.A., Sharman, G.R., Graham, S.A., Fildani, A., 2015. Characterization and diachronous initiation of coarse clastic deposition in the Magallanes-Austral foreland basin, Patagonian Andes. Basin Res. 29, 298–326.

Malkowski, M.A., Schwartz, T., Sharmann, G.R., Sickmann, Z.T., Graham, S.A., 2017. Stratigraphic and Provenance Variations in the Early Evolution of the Magallanes-

Austral Foreland Basin: Implications for the Role of Longitudinal versus Transverse Sediment Dispersal during Arc-Continent Collision, vol. 129. Geological Society of America Bulletin, pp. 349–371.

Manassero, M.J., 1988. Petrología y procedencia de las areniscas cretácicas superiores de la Cuenca Austral Argentina. Rev. Asoc. Geol. Argent. 18, 175–187.

Marfil, R., Delgado, A., Rossi, C., La Iglesia, A., Ramseyer, K., 2003. Origin and diagenetic evolution of kaolin in reservoir sandstones and associated shales of the Jurassic and Cretaceous, Salam Fields, Western Desert (Egypt). In: Worden, R.H., Morad, S. (Eds.), Quartz Cementation in Sandstones, Clay Mineral Cement in Sandstones: International Association of Sedimentologists, vol. 34. Special Publication, pp. 319–342.

Middelburg, J.J., Van Der Weijden, C.H., Woittiez, J.R.W., 1988. Chemical processes affecting the mobility of major, minor and trace elements during weathering of granitic rocks. Chem. Geol. 68 (3–4), 253–273.

Moore, D.M., Reynolds, J.R.R.C., 1989. X-Ray Diffraction and the Identification and Analysis of Clay Mineral. Oxford University Press, p. 329.

Moore, D.M., Reynolds Jr., R.C., 1997. X-ray Diffraction and the Identification and Analysis of Clay Minerals. Oxford University Press, Oxford.

Moore, W.R., Zee Ma, Y., Piriem, I., Zhang, Y., 2016. Thight gas sandstone reservoirs, Part 2: Petrophysical analysis and reservoir modeling. In: Zee, Y., Holditch, S.A. (Eds.), Unconventional Oil and Gas Resources Handbook, pp. 429–448.

Morad, S., Ketzer, J.M., De Ros, F.L., 2000. Spatial and temporal distribution of diagenetic alterations in siliciclastic rocks: implications for mass transfer in sedimentary basins. Sedimentology 47, 95–120.

Morad, S., Al-Ramadam, K., Ketzer, M., De Ros, L.F., 2010. The impact of diagenesis on the heterogeneity of sandstone reservoirs: a review of the role of depositional fades and sequence stratigraphy. American Assoc. Petrol. Geol. 94 (8), 1267–1309.

Moraes, M.A.S., Surdam, R.C., 1993. Diagenetic heterogeneity and reservoir quality: fluvial, deltaic, and turbiditic sandstone reservoirs, Potiguar and Recôncavo rift basins, Brazil. AAPG (Am. Assoc. Pet. Geol.) Bull. 77, 1142–1158.

Moyano-Paz, D., Tettamanti, C., Varela, A.N., Cereceda, A., Poiré, D.G., 2018. Depositional processes and stratigraphic evolution of the Campanian deltaic system of La Anita Formation, Austral-Magallanes Basin, patagonia, Argentina. Lat. Am. J. Sedimentol. Basin Anal. 26 (2), 155–166.

Moyano-Paz, D., Richiano, S., Varela, A.N., Gómez-Dacal, A.R., Poiré, D.G., 2020. Ichnological signatures from wave- and fluvial-dominated deltas: the La Anita Formation, upper Cretaceous, Austral-Magallanes Basin. Patagonia: Mar. Petrol. Geol. 114, 104168.

Moyano-Paz, D., Rozadilla, S., Agnolin, F., Vera, E., Coronel, M.D., Varela, A.N., Gómez-Dacal, A.R., Aranciaga-Rolando, A.M., D`Angelo, J.S., Pérez-Loinaze, V., Richiano, S., Chimento, N.R., Motta, M.J., Sterli, J., Manabe, M., Takanobu, T., Isasi, M.P., Poiré, D.G., Novas, F.E., 2022. The uppermost Cretaceous continental deposits (UCCD) at southern end of patagonia, the Chorrillo formation case study (Austral-Magallanes Basin): Sedimentology, fossil content and regional implications. Cretac. Res. https://doi.org/10.1016/j.cretres.2021.105059.

Nabawy, B.S., Géraud, Y., 2015. Impacts of pore- and petro-fabrics, mineral composition and diagenetic history on the bulk thermal conductivity of sandstones. J. Afr. Earth Sci. 115, 21–24.

Natland, M.L., Gonzalez, P.E., Canon, A., Ernst, M., 1974. A System of Stages for Correlation of Magallanes Basin Sediments, vol. 139. American Association of Petroleum Geologists Memoir, p. 129.

Net, L., Limarino, C.O., 2000. Caracterización y origen de la porosidad en areniscas de la sección inferior del Grupo Paganzo (Carbonífero superior), Cuenca Paganzo, Argentina. Lat. Am. J. Sedimentol. Basin Anal. 7, 49–72.

Nesbitt, H.W., Young, G.M., 1982. Early Proterozoic climates and plate motions inferred from major element chemistry of lutites. Nature 229, 715–717.

Net, L., Alonso, S., Limarino, C.O., 2002. Source rock and environmental control on clay mineral associations, Lower section of Paganzo Group (Carboniferous), North-west Argentina. Sediment. Geol. 152, 183–199.

Nie, J., Horton, B.K., Saylor, J.E., Mora, A., Mange, M., Garzione, C.N., Basu, A., Moreno, C.J., Caballero, V., Parra, M., 2012. Integrated provenance analysis of a convergent retroarc foreland system: U-Pb ages, heavy minerals, Nd isotopes, and sandstone compositions of the Middle Magdalena Valley basin, northern Andes, Colombia. Earth Sci. Rev. 110, 111–126.

O'Brien, C.L., Robinson, S.A., Pancost, R.D., Sinninghe Damsté, J.S., Schouten, S., Lunt, D.J., Alsenz, H., Bornemann, A., Bottini, C., Brassell, S.C., Farnsworth, A., Forster, A., Huber, B.T., Inglis, G.N., Jenkyns, H.C., Linnert, C., Littler, K., Markwick, P., Mcanena, A., Mutterlose, J., Naafs, B.D.A., Püttmann, W., Sluijs, A., Van Helmond, A.G.M., Vellekoop, J., Wagner, T., Wrobel, N.E., 2017. Cretaceous sea-surface temperature evolution: constraints from TEX86 and planktonic foraminiferal oxygen isotopes. Earth Sci. Rev. 172, 224–247.

O'Connor, L.K., Robinson, S.A., Naafs, B.D.A., Jenkyns, H.C., Henson, S., Clarke, M., Pancost, R.D., 2019. Late Cretaceous temperature evolution of the southern high latitudes: a TEX86 perspective. Paleoceanogr. Paleoclimatol. 34, 436–445.

Odin, G.S., 1985. Significance of green particles (glaucony, berthierine, chlorite) in arenites. In: Zuffa, G.G. (Ed.), Provenance of Arenites: NATO-Advanced Study Institute Series C: Mathematical and Physical Sciences, vol. 148. Reidel Publishing Co., Dordrecht, Netherlands, D, pp. 279–307.

Odin, G.S., 1990. Clay mineral formation at the continent-ocean boundary: the verdine facies. Clay Miner. 25, 477–483.

Odino, A.L., Gómez-Peral, L.E., Richiano, S., Macchioli Grande, M., Borya, A., Poiré, D. G., Bahniuk, A.M., Cury, L.F., 2021. Geochemical and mineralogical evidence of an offset in the Andean arc recorded in the Upper Cretaceous marine deposits of the Austral-Magallanes basin, Argentina. J. S. Am. Earth Sci. 111, 103426.

Packer, B.M., Ingersoll, R.V., 1986. Provenance and petrology of deep sea drilling project sands and sandstones from the Japan and mariana Forearc and backarc basins. Sediment. Geol. 51, 5–28.

Pankhurst, R.J., Riley, T.R., Fanning, C.M., Kelley, S.P., 2000. Episodic silicic volcanism in patagonia and Antarctic Peninsula: Chronology of magmatism associated with the break-up of Gondwana. J. Petrol. 41, 605–625.

Pettijohn, F.J., Potter, P., Siever, R., 1972. Sand and Sandstone, first ed. Springer-Verlag, Berlin, p. 618.

Raigemborn, M.S., Gómez-Peral, L.E., Krause, J.M., Matheos, S.D., 2014. Controls on clay minerals assemblages in an early Palaeogene nonmarine succession: implications for the volcanic and paleoclimatic record of extra-andean patagonia, Argentina. J. S. Am. Earth Sci. 52, 1–23.

Ramos, V.A., Niemeyer, H., Skarmeta, J., Muñoz, J., 1982. Magmatic evolution of the Austral Patagonian Andes. Earth Sci. Rev. 18, 411–443.

Richiano, S., Varela, A.N., Gomez Peral, L.E., Cereceda, A., Poiré, D.G., 2015. Composition of the lower Cretaceous source rock from the Austral basin (Río mayer formation, patagonia, Argentina): regional implication for unconventional reservoirs in the southern Andes. Mar. Petrol. Geol. 66, 764–790.

Robinson, S., Heimhofer, U., Hesselbo, S.P., Petrizzo, M.R., 2017. Mesozoic climates and oceans – a tribute to hugh Jenkyns and helmut Weissert. Sedimentology 64, 1–15.

Romans, B.W., Fildani, A., Hubbard, S.M., Covault, J.A., Fosdick, J.C., Graham, S.A., 2011. Evolution of deep-water stratigraphic architecture. Magallanes Basin, Chile: Mar. Petrol. Geol. 28, 612–628.

Santamarina, P.E., Barreda, V.D., Moyano-Paz, D., Tettamanti, C., Iglesias, A., Poiré, D. G., Varela, A.N., 2020. Palynoflora from the La Anita Formation (Maastrichtian), Austral-Magallanes Basin. Argentina Rev. Mus. Argent. Ciencias Nat. Nueva Ser. 22 (1), 47–56.

Schultz, L.G., 1964. Quantitative Interpretation of Mineralogical Composition from X-Ray and Chemical Data for Pierra Shale: U.S, vol. 391. Geological Survey Professional Paper, pp. 1–31.

Senkayi, A.L., Ming, D.W., Dixon, J.B., Hossner, L.R., 1987. Kaolinite, opal CT, and clinoptilolite in altered tuffs interbedded with lignite in the Jackson Group. Texas Clay Clay Miner. 35, 281–290.

Shalaby, M.R., Hakimi, M.H., Abdullah, W.H., 2012. Geochemical characterization of solid bitumen (migrabitumen) in the Jurassic sandstone reservoir of the Tut field, Shushan basin, northern western desert of Egypt. Int. J. Coal Geol. 100, 26–39.

Shanmugam, G.S., 2012. New perspectives on deep-water sandstone: origin, recognition, initiation, and reservoir quality. In: Handbook of Petroleum Exploration and Production, vol. 9. Elsevier, Amsterdam, p. 524.

Sickmann, Z.T., Schwartz, T.M., Malkowski, M.A., Dobbs, S.C., Graham, S.A., 2019. Interpreting Large Detrital Geochronology Data Sets in Retroarc Foreland Basins: an Example from the Magallanes-Austral Basin. https://doi.org/10.1130/L1060.1 southernmost Patagonia: Lithosphere.

Spalletti, L.A., Matheos, S.D., Sánchez, E., Oyarzábal, F., 2005. Análisis diagenético de la Formación Springhill (Santa Cruz, Argentina): VI Congreso de Exploración y Desarrollo de Hidrocarburos. Mar del Plata, CD Actas, p. 14.

Stefani, C., Fellin, M.G., Zattin, M., Zuffa, G., Dalmonte, C., Mancin, N., Zanferrari, A., 2007. Provenance and paleogeographic evolution in a multi-source foreland: the Cenozoic Venetian–Friulian Basin (NE Italy). J. Sediment. Res. 77, 867–887.

Suczek, C.A., Ingersoll, R.A., 1985. Petrology and provenance of Cenozoic sand from the Indus cone and Arabian basin, DSDP sites 221, 222 and 224. J. Sediment. Petrol. 55, 340–346.

Surdam, R.C., Jiao, Z.S., Heasler, H.P., 1997. Anomalously pressured gas compartments in Cretaceous rocks of the Laramide basins of Wyoming: a new class of hydrocarbon accumulation. In: Surdam, R.C. (Ed.), Seals, Traps, and the Petroleum Systems, vol. 67. American Association of Petroleum Geologists Memoir, pp. 199–222.

Taylor, R.T., Giles, M.R., Hathon, L.A., Diggs, T.N., Braunsdorf, N.R., Birbiglia, G.V., Kittridge, M.G., Macaulay, C.I., Espejo, I.S., 2010. Sandstone diagenesis and reservoir quality prediction: models, myths, and reality. AAPG (Am. Assoc. Pet. Geol.) Bull. 94, 1093–1132.

Tettamanti, C., Moyano-Paz, D., Varela, A.N., Gómez-Peral, L.E., Poiré, D.G., Cereceda, A., Odino, A.L., 2018. Sedimentology and stratigraphy of the uppermost Cretaceous continental deposits of the Austral-Magallanes Basin, patagonia, Argentina. Lat. Am. J. Sedimentol. Basin Anal. 25 (2), 149–168.

Thiry, M., 2000. Palaeoclimatic interpretation of clay minerals in marine deposits: an outlook from the continental origin. Earth Sci. Rev. 49, 201–221.

Varela, A.N., Poire, D.G., Martin, T., Gerdes, A., Goin, F.J., Gelfo, J.N., Hoffmann, S., 2012. U-Pb zircon constraints on the age of the Cretaceous Mata Amarilla formation, southern patagonia, Argentina: its relationship with the evolution of the Austral basin. Andean Geol. 39, 359–379.

Varela, A.N., Gomez Peral, L.E., Richiano, S., Poire, D.G., 2013. Distinguishing similar volcanic source areas from an integrated provenance analysis: implications for foreland Andean basin. J. Sediment. Res. 83, 258–276.

Varela, A.N., Raigemborn, M.S., Richiano, S., White, T., Poiré, D.G., Lizzoli, S., 2018. Late Cretaceous paleosols as paleoclimate proxies of high-latitude southern hemisphere: Mata Amarilla formation, patagonia, Argentina. Sediment. Geol. 363, 83–95.

Varela, A.N., Richiano, S., D'Elia, L., Moyano-Paz, D., Tettamanti, C., Poiré, D.G., 2019. Sedimentology and stratigraphy of the Puesto El Moro formation, patagonia, Argentina: implications for upper Cretaceous paleogeographic reconstruction and compartmentalization of the Austral- Magallanes Basin. J. S. Am. Earth Sci. 92, 466–480.

Wanas, H.A., Assal, E.M., 2021. Provenance, tectonic setting and source area-paleoweathering of sandstone of the Bahariya Formation in the Bahariya Oasis,

Egypt: an implication to paleoclimate and paleogeography of the southern Neo-Tethys region during Early Cenomanian. Sediment. Geol. 413, 105822.

Wilhelms, A., Larter, S.R., 1995. Overview of the geochemistry of some tar mats from the North Sea and U.S.A.: Implications for tar-mat origin. In: Cubitt, J.M., England, W.A. (Eds.), The Geochemistry of Reservoirs, vol. 88. Geological Society Special Publication, pp. 87–101.

Wilson, T.J., 1991. Transition from Back-Arc to Foreland Basin Development in Southernmost Andes: Stratigraphic Record from the Ultima Esperanza District, Chile, vol. 103. Geological Society of America, Bulletin, pp. 98–111.

Wilson, M.D., Pittman, E.D., 1977. Authigenic clays in sandstones: recognition and influence on reservoir properties and paleoenvironmental analysis. J. Sediment. Petrol. 47, 3–31.

Worden, R.H., Morad, S., 2000. Quartz cementation in oil field sandstones: a review of the key controversies. In: Worden, R.H., Morad, S. (Eds.), Quartz Cementation in Sandstones: International Association of Sedimentologists, vol. 29. Special Publication, pp. 1–20.

Worden, R., Morad, S., 2003. Clay minerals in sandstones: Controls on formation, distribution and evolution. In: Worden, R.H., Morad, S. (Eds.), Clay Cements in Sandstones, vol. 34. International Association of Sedimentologists Special Publication, pp. 3–41.

Xu, T., Wang, X., Zhang, Y., Zhao, X., Bao, Y., 2003. Clay Minerals in Sedimentary Basins of China. Petroleum Industry Press, Beijing, p. 65.

Yasin, M., Ibrahim, M., 2017. X-ray diffraction analysis for the interpretation of clay minerals paragenesis in the Neogene sediments of Mang and vicinity, Sub-Himalayas, Pakistan. Earth Sci. Malaysia 1 (1), 32–35.

Zahid, K.M., Barbeau Jr., D.L., 2011. Constructing sandstone provenance and classification ternaty diagrams using an electronic spreadsheet. J. Sediment. Res. 81, 702–707.

Zattin, M., Stefani, C., Martin, S., 2003. Detrital fission-track analysis and petrography as keys of Alpine exhumation: the example of the Veneto foreland (Southern Alps, Italy). J. Sediment. Res. 73, 1051–1061.

Zhang, L., Bai, G., Luo, X., Ma, X., Chen, M., Wu, M., Yang, W., 2009. Diagenetic history of tight sandstones and gas entrapment in the Yulin Gas Field in the central area of the Ordos Basin. China Mar. Petrol. Geol. 26, 974–989.

Zhao, J., Wu, S., Wu, F., 2007. The classification and evaluation criteria for low permeability reservoirs: an example from the Ordos Basin. Lithologic Reservoirs 19 (3), 28–34.

Zou, C., Zhang, G., Tao, S., 2010. Geological Features and Exploration Discoveries of Unconventional Resources and the Petroleum Geological Theory, vol. 37. Petroleum Exploration and Development, pp. 129–145.

Zou, C., Zhu, R., Liu, K., Su, L., Bai, B., Zhang, X., Yuan, X., Wang, J., 2012. Tight gas sandstone reservoirs in China: characteristics and recognition criteria. J. Petrol. Sci. Eng. 88 (89), 82–91.